EDGE ARTICLE

Check for updates

Monitoring phagocytic uptake of amyloid β into glial cell lysosomes in real time†

Priya Prakash, [ID] ‡[a] Krupal P. Jethava, [ID] ‡[a] Nils Korte, [ID] ‡[b] Pablo Izquierdo, [ID] ‡[b] Emilia Favuzzi,[cd] Indigo V. L. Rose, [ID][e] Kevin A. Guttenplan, [ID][f] Palak Manchanda, [ID][a] Sayan Dutta,[g] Jean-Christophe Rochet, [ID][gh] Gord Fishell,[cd] Shane A. Liddelow, [ID][eij] David Attwell [ID][b] and Gaurav Chopra [ID]*[ahklm]

Phagocytosis by glial cells is essential to regulate brain function during health and disease. Therapies for Alzheimer's disease (AD) have primarily focused on targeting antibodies to amyloid β (Aβ) or inhibitng enzymes that make it, and while removal of Aβ by phagocytosis is protective early in AD it remains poorly understood. Impaired phagocytic function of glial cells during later stages of AD likely contributes to worsened disease outcome, but the underlying mechanisms of how this occurs remain unknown. We have developed a human $Aβ_{1-42}$ analogue ($Aβ^{pH}$) that exhibits green fluorescence upon internalization into the acidic organelles of cells but is non-fluorescent at physiological pH. This allowed us to image, for the first time, glial uptake of $Aβ^{pH}$ in real time in live animals. We find that microglia phagocytose more $Aβ^{pH}$ than astrocytes in culture, in brain slices and in vivo. $Aβ^{pH}$ can be used to investigate the phagocytic mechanisms responsible for removing Aβ from the extracellular space, and thus could become a useful tool to study Aβ clearance at different stages of AD.

Introduction

Glial cells make up more than half of the cells of the central nervous system (CNS) and are vital to the regulation of brain function.[1] Microglia are specialized CNS-resident macrophages that respond to pathogens and injury by clearing cell debris, misfolded protein aggregates and damaged neurons by the process of phagocytosis.[2] Mature microglia in the adult brain exhibit a ramified morphology and constantly survey their surroundings for "eat me" signals[3] present on or released from apoptotic cells, microbes, protein deposits, dysfunctional synapses and other target substrates. After CNS injury or during neurodegenerative diseases like Alzheimer's disease (AD) microglia become "reactive", and change morphology,

becoming rod-like or amoeboid,[4] and actively engage with their environment by secreting inflammatory cytokines like TNF-α and IL-1α/β. These cytokines cause functional changes in astrocytes, microglia themselves, and other cells.[5,6]

During phagocytosis, proteins on the microglial cell surface, such as the Toll-Like Receptors (TLRs), Fc receptors, and scavenger receptors including CD36 and the receptor for advanced glycation end products (RAGE) among others, recognize the "eat-me" signals and engulf the target substrates into intracellular compartments called phagosomes.[7–10] The phagosomes mature by fusing with lysosomes to form highly acidic phagolysosomes and mobilize the phagocytosed material for enzymatic degradation. The pH of phagosomal organelles during this maturation process is progressively reduced[11] from 6.0 to

[a]Department of Chemistry, Purdue University, West Lafayette, IN 47907, USA. E-mail: gchopra@purdue.edu

[b]Department of Neuroscience, Physiology and Pharmacology, University College London, London WC1E 6BT, UK

[c]Department of Neurobiology, Harvard Medical School, 220 Longwood Avenue, Boston, MA 02115, USA

[d]Stanley Center at the Broad, 75 Ames Street, Cambridge, MA 02142, USA

[e]Neuroscience Institute, NYU Grossman School of Medicine, New York, NY 10016, USA

[f]Department of Neurobiology, Stanford University, Stanford, CA 94305, USA

[g]Department of Medicinal Chemistry and Molecular Pharmacology, Purdue University, West Lafayette, IN 47907, USA

[h]Purdue Institute for Integrative Neuroscience, Purdue University, West Lafayette, IN 47907, USA

[i]Department of Neuroscience & Physiology, NYU Grossman School of Medicine, New York, NY 10016, USA

[j]Department of Ophthalmology, NYU Grossman School of Medicine, New York, NY 10016, USA

[k]Purdue Institute for Drug Discovery, 720 Clinic Drive, West Lafayette, IN 47907, USA

[l]Purdue Center for Cancer Research, Purdue University, West Lafayette, IN 47907, USA

[m]Purdue Institute of Inflammation, Immunology and Infectious Disease, Purdue University, West Lafayette, IN 47907, USA

† Electronic supplementary information (ESI) available: Instrumentation, detailed chemical characterization of $Aβ^{pH}$ (MALDI-MS, ^{1}H-NMR, FTIR), movies, flow cytometry, and confocal microscopy supporting data. See DOI: 10.1039/d1sc03486c

‡ These authors contributed equally to this work.

around 5.0–4.5. Although microglia are the "professional phagocytes" of the CNS, astrocytes are also competent phagocytic cells with important roles both during health, and in response to injury or in disease.[12–15] Recent evidence has demonstrated the phagocytic abilities of reactive astrocytes towards cellular debris in CNS injury.[16] Together, reactive microglia and astrocytes play a crucial role in clearing extracellular debris and cellular components and aid in remodeling the tissue environment during disease.

AD is characterized by the generation of soluble oligomers of amyloid β (Aβ) that have numerous downstream actions, including reducing cerebral blood flow,[17] inhibiting glutamate uptake which may cause hyperexcitability of neurons,[18] and inducing hyperphosphorylation of the cytoskeletal protein tau[19,20] which leads to synaptic dysfunction and cognitive decline. Ultimately Aβ oligomers are deposited as extracellular plaques in the brain, a hallmark of AD, which contribute to neuroinflammation and neuronal death.[21] The main Aβ species generated excessively in AD is Aβ$_{1-42}$, which is a small ~4.5 kDa peptide produced by the cleavage of amyloid precursor protein on neuronal membranes by β- and γ-secretases.[22,23] Removal of Aβ from the extracellular space by phagocytosis into microglia and astrocytes, as well as by clearance across endothelial cells into the blood or lymph vessels, is thought to limit the build-up of the extracellular Aβ concentration. However, AD pathology occurs when Aβ generation outweighs its removal.[20] Thus, to understand the onset of plaque deposition during AD (and perhaps how to prevent it) it is essential to understand molecular mechanisms underlying glial phagocytosis and degradation of Aβ. A method that can monitor this process, especially in real time *in vivo*, will facilitate identification of the receptors that bind to Aβ and initiate its phagocytic clearance. This will allow investigation of why glia that surround Aβ plaques in AD show impaired phagocytic function,[5,24,25] and why in inflammatory conditions microglia may increase their phagocytic capacity depending on their state of activation.[26,27]

Current methods to study glial phagocytosis involve the use of fluorescent latex beads,[28] particles of zymosan,[29] or *E. coli*[30] conjugated to fluorophores like fluorescein and rhodamine.[31] A non-pH dependent particle makes it difficult to clearly determine whether the particle is inside the phagosomes or outside the cell during live-cell monitoring (Fig. S1A†). Some bioparticles can be labeled with pH-sensitive dyes such as pHrodo, however, these currently available pH-sensitive dyes are not suitable for labeling disease-specific pathogenic molecules like Aβ for *in vivo* use. While non-pH sensitive fluorophore conjugates of Aβ have been used to evaluate Aβ phagocytosis,[28,32] they have several disadvantages for live-cell imaging and cannot be used for selective identification and isolation of phagocytic cells *in vivo*. First, acidic pH-insensitive fluorophore-conjugated Aβ peptides exhibit sustained fluorescence in the extracellular space (at physiological pH) thus contributing a noisy background that hinders the clear visualization of live phagocytic cells (Fig. S1B†). Second, in live-cell imaging and in fluorescence-activated cell sorting (FACS) of live cells, it is difficult to differentiate between Aβ molecules that are

internalized by the cells *versus* Aβ molecules that are stuck to the cell surface.

To address these issues, we have developed a pH-dependent fluorescent conjugate of human Aβ$_{1-42}$, which we call Aβ^{pH}, and characterized it using mass spectrometry, atomic force microscopy and imaging of its uptake into cells *in vitro* and *in vivo*. We show the functionality of the Aβ^{pH} probe for identifying phagocytic microglia and astrocytes in several different biological model systems such as cell lines, primary cell cultures, brain tissue slices, and *in vivo* in brain and retina. Aβ^{pH} retains an aggregation phenotype similar to that of synthetic Aβ *in vitro* and exhibits increased green fluorescence within the acidic pH range of 5.0 to 4.5 but not at the extracellular and cytoplasmic physiological pH values of 7.4 and 7.1, respectively. Aβ^{pH} can be used to visualize phagocytosis in live cells in real time without the use of any Aβ-specific antibody. It is internalized by glial cells (both astrocytes and microglia) in live rat hippocampal tissue sections *in situ*. Stereotaxic injection of Aβ^{pH} into the mouse somatosensory cortex *in vivo* leads to its uptake by astrocytes and microglia, following which microglia retain the Aβ^{pH} within the cells up to 3 days *in vivo* unlike astrocytes. Similarly, microglia in retinal tissues retain the Aβ^{pH} within the cells for up to 3 days but no signal was detected in astrocytes. Finally, we show, for the first time, real-time phagocytosis of Aβ into microglia and astrocytes in mouse cortex *in vivo* by two-photon excitation microscopy.

Results

Properties of a novel pH-dependent fluorescent conjugate of human Aβ$_{1-42}$

We synthesized a new pH-sensitive fluorescent dye-labelled phagocytic Aβ probe for imaging both *in vitro* and *in vivo*, and for cell sorting which allows for downstream analysis of functional subtypes of cells. We used a facile bioconjugation strategy to make our new probe safe for use with live cells *in vitro* and with live animals *in vivo*. The Aβ^{pH} conjugate was synthesized at the microgram scale by linking the synthetic human Aβ$_{1-42}$ peptide to the amine-reactive Protonex Green 500, SE (PTXG) fluorophore (Fig. 1A). We selected PTXG based on its ability to gain fluorescence in acidic environments and thus emit fluorescence specifically at the low pH of 5.0–4.5 found within lysosomes – a property of only a few commercial dyes. Conjugation of the fluorophore was performed at the side chain amine groups of the lysine residues within, and at the N-terminal of, human Aβ$_{1-42}$ peptide. The conjugation was confirmed with matrix-assisted laser desorption/ionization-mass spectrometry (MALDI-MS) (Fig. S2A and B†) that indicated the conjugation of PTXG with the Aβ$_{1-42}$ peptide (molecular weight >4.5 kDa) by removal of succinimidyl ester (SE) as a leaving group. Additionally, proton nuclear magnetic resonance (^{1}H-NMR) analysis of Aβ^{pH} also demonstrated the presence of PTXG as well as Aβ$_{1-42}$ peptide (Fig. S3A–C†). The spectrum of Aβ$_{1-42}$ peptide obtained from attenuated total reflection Fourier transform infrared spectroscopy (ATR-FTIR) also shows a strong absorption peak at 1625 cm^{-1} confirming carbonyl functional group of amide bonds (Fig. S4A†) and the
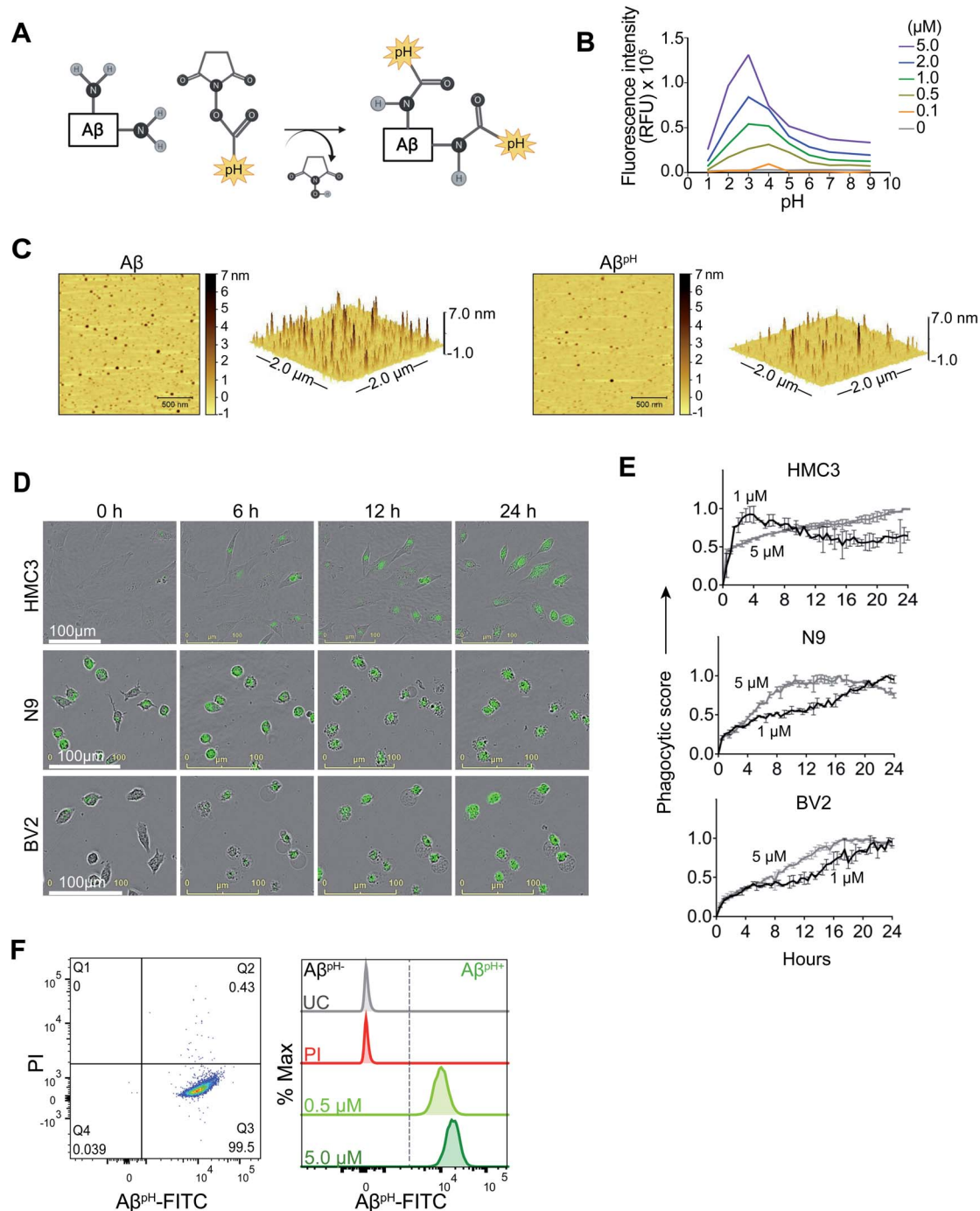
Fig. 1 Synthesis and characterization of Aβ^{pH}. (A) The Aβ^{pH} is synthesized by conjugating the amine-reactive pH-sensitive Protonex Green dye to the side chain amine groups of the lysine residues and the N-terminal of human Aβ$_{1-42}$ peptide. (B) The pH-sensitivity of the Aβ^{pH} probe characterized at different concentrations from 0.1 μM to 5.0 μM. Increased fluorescence is observed at acidic pH values of ~5.0 to ~2.0, covering the pH range of the intracellular acidic organelles. (C) Atomic force microscopy topographic images of Aβ^{pH} oligomers compared to synthetic Aβ oligomers. Left-2D topographic image of Aβ^{pH} and synthetic Aβ oligomers. Right-3D image (2 × 2 μm $x-y$). (D) Live cell imaging of the phagocytic uptake of 1 μM Aβ^{pH} by BV2 and N9 mouse microglia and by HMC3 human microglia over 24 hours. (E) Quantification of Aβ^{pH} phagocytic score by BV2, N9, and HMC3 microglial cells from the live cell images. (F) The phagocytic uptake of Aβ^{pH} by BV2 cells is measured and quantified *via* flow cytometry analysis. Dot plot shows live (PI^{-}) and Aβ^{pH+} cells. No green fluorescence is measured in unstained cells (UC) and in dead cells stained with the PI only whereas green fluorescence is measured in cells treated with 0.5 and 5.0 μM Aβ^{pH} for 1 hour (higher fluorescence is seen in cells exposed to the higher concentration of Aβ^{pH}). Data shown in terms of % max, by scaling each curve to mode = 100% (y-axis).

spectrum of PTXG shows the presence of amide and ester group with absorption peaks at 1668 and 1727 cm^{-1}, respectively (Fig. S4B†). The conjugated product Aβ^{PH} shows a distinct peak at 1674 cm^{-1} confirming amide bond formation between the Aβ$_{1-42}$ peptide and PTXG dye, as expected (Fig. S4C†). Collectively, these experiments confirm the formation of the peptide–dye conjugate. We also synthesized another conjugate of Aβ$_{1-42}$ with the pHrodo-Red, NHS fluorophore (RODO) and confirmed conjugate formation from the MALDI-MS spectrum (Fig. S5†).

The pH-sensitivity of the PTXG and RODO-conjugated Aβ was assessed by measuring their fluorescence intensities at various pH values. Notably, the pK_a of a dye may shift when conjugated with a protein or peptide and this would change the pH-sensitivity of the conjugated product.[33] At the concentrations of 0.5, 1.0, 2.0, and 5.0 μM, the PTXG-conjugated Aβ showed increased fluorescence at pH less than ~5.5 whereas PTXG alone showed increased fluorescence at pH ~4.5 with excitation/emission wavelengths of 443/505 nm. The pK_a of PTXG-conjugated Aβ was 5.2–5.9 and the pK_a of PTXG alone was 4.4–4.7 at concentrations of 0.5, 1.0, 2.0 and 5.0 μM (Fig. S6A†). The PTXG dye clearly shows increased fluorescence around pH ~4.5 whereas PTXG-conjugated Aβ shows a pK_a of ~5.5 that lies within the pH range of lysosomes thus making it suitable for our study. On the other hand, the RODO-conjugated Aβ had a pK_a value of 6.2–6.4 at four concentrations (5, 2, 1, 0.5 μM) (Fig. S6B†). It is known that the amine-reactive forms of the RODO dye have a pK_a of ~7.3 in solution and shift to about ~6.5 upon conjugation[34] which is similar to the pK_a value we observed for RODO-conjugated Aβ. Furthermore, the PTXG–Aβ conjugate showed a maximum fluorescence intensity between 500 and 510 nm in the acidic pH range that covers the pH values of the lysosomal organelles (Fig. S7A†). The PTXG–Aβ conjugate exhibited low fluorescence intensity at pH values more alkaline than 6.0 including at the physiological extracellular pH of 7.4. In contrast, the RODO-conjugated Aβ does not show a consistent pattern of higher florescence at similar acidic pH range and the pattern of pH sensitivity is dependent on concentration (Fig. S7B†). Overall, these experiments show that the pK_a shifts towards phagosomal pH range when PTXG is conjugated to Aβ (average pK_a ~5.5) compared to the value for PTXG alone (average pK_a ~4.5) whereas RODO-conjugated Aβ has a pK_a of ~6.3 that is more alkaline and close to the endosomal pH range of around 6.4–6.5.[35] We also tested to see if the unconjugated PTXG and RODO dyes were endogenously taken up by the cells. BV2 microglia treated with PTXG alone showed very low fluorescence indicating minimal uptake of the dye compared to cells treated with the PTXG–Aβ conjugate. The cells treated with RODO alone showed high fluorescence indicating higher dye uptake (at 1 μM, the cells showed almost 50% fluorescence with RODO compared to the RODO–Aβ conjugate) (Fig. S8†) limiting its *in vivo* use. Neither of the two dyes were toxic to the cells in culture (Fig. S9†).

In order to validate that the PTXG–Aβ fluorescence increase is due to the acidic environment of the phagosome, we measured the fluorescence of the PTXG–Aβ conjugate in cells treated with bafilomycin A (BF), a compound that inhibits lysosomal acidification by blocking phagosome–lysosome

fusion during late stages of phagocytosis.[36] As expected, we measured a decrease in cellular PTXG–Aβ fluorescence with BF treatment compared to the control cells (Fig. S10†). The reduction in PTXG–Aβ fluorescence in the presence of BF indicates that the fluorescence of PTXG–Aβ is dependent on the acidic pH of the lysosomal organelles. Thus, summarizing the above-experiments, we believe that the PTXG–Aβ conjugate outperforms the RODO–Aβ conjugate due to the following reasons: (i) a narrower range of fluorescence, (ii) minimal background uptake, (iii) the long-term sustained fluorescence intensity of PTXG–Aβ (Fig. S11†), and (iv) a more suitable pK_a value. Thus, the PTXG–Aβ conjugate performed better and was chosen for all further experiments (termed Aβ^{PH} henceforth in the paper). Lastly, we wanted to determine whether Aβ^{PH} exhibits aggregation properties similar to the aggregation of synthetic, non-conjugated Aβ. The Aβ$_{1-42}$ and Aβ^{PH} oligomers were prepared[37] from hexafluoroisopropanol (HFIP) treated peptide films in PBS pH 7.4 buffer at 4 °C. Atomic force microscopy (AFM) revealed that the ability of Aβ^{PH} to aggregate is similar, in size and height, to that of the non-conjugated Aβ (Fig. 1C) suggesting that Aβ^{PH} is suitable for biological use.[38,39]

Aβ^{PH} uptake into human and mouse microglial cell lines

To visualize phagocytosis of Aβ^{PH} in real time in live microglial cells, immortalized human microglial clone 3 (HMC3) cells and mouse BV2 and N9 microglial cells were treated with 1, 2 and 5.0 μM concentrations of Aβ^{PH} and live-cell images were acquired every 30 minutes for 24 hours (Fig. 1D). We observed internalization and increased fluorescence of Aβ^{PH} (implying phagocytosis) by HMC3 cells. The fluorescence was quantified as a phagocytic score, *i.e.* relative fluorescence compared to initial time ($t = 0$) normalized over the 24 hour period (see Methods). For HMC3 cells there was an initial rapid phase of fluorescence (score) increase followed either by a slower increase in fluorescence at 5 μM Aβ^{PH} concentration or a slow decrease of fluorescence from its peak value at 1 μM and 2 μM Aβ^{PH} concentration (Fig. 1E and S12†). This suggests rapid initial uptake of Aβ^{PH}, followed by intracellular degradation of Aβ^{PH} which occurs either more rapidly than the influx (giving a slow decline) or less rapidly than the influx (giving a slowed increase) (Fig. S12†). Cells that did not phagocytose Aβ^{PH} did not display any green fluorescence thereby differentiating Aβ^{PH}-specific phagocytic and non-phagocytic microglial cells in real time. Rodent microglial cell lines (BV2 and N9) showed a peak of phagocytic score at 12–16 hours for N9 and 16–20 hours for BV2 at 5 μM Aβ^{PH} treatment, compared to the HMC3 human microglial cell line that showed a gradual increase in phagocytosis over the 24 hour treatment period for the same concentration. Interestingly, for the lower Aβ^{PH} doses of 1 μM and 2 μM, the peak value of phagocytic score for HMC3 cells was within the initial 4 hours compared to the gradual increase for the rodent cell lines over the 24 hour period (Fig. S12†). Using live-cell imaging, we also observed interesting morphological differences over time between phagocytic and non-phagocytic microglial cells. During the initial 2 hours, many cells displayed an elongated, branched morphology followed by

acquisition of an amoeboid morphology during subsequent time points when phagocytosis was occurring, as indicated by increased fluorescence (Movies S1–S3†). Thus, the $A\beta^{PH}$ reporter can be used to visualize $A\beta$-specific phagocytosis in real-time and can be used in experiments to evaluate enhancement or inhibition of microglial phagocytosis for *in vitro* screening of drug candidates for AD.

Flow cytometry of $A\beta^{PH}$ phagocytic cells and staining of $A\beta^{PH}$ after phagocytosis in fixed primary cultured microglia and astrocytes

We next determined whether $A\beta^{PH}$ can be used to analyze phagocytosing cells using flow cytometry. By adding $A\beta^{PH}$ to BV2 cells *in vitro*, we show that live microglial cells that phagocytose $A\beta^{PH}$ can be easily analyzed with flow cytometry without the need for traditional dyes or antibodies to detect $A\beta$ (Fig. 1F and S13A†). Phagocytic uptake of $A\beta^{PH}$ by BV2 microglia was evident with a green fluorescence peak within live cells when the cells were treated with 0.5 μM and 5.0 μM $A\beta^{PH}$ for 1 hour in culture, with unstained and live/dead stained cells as controls. There was a slight increase in $A\beta^{PH}$ fluorescence at 1 hour when the $A\beta^{PH}$ concentration was increased 10-fold. The green fluorescence signal indicates internalization of $A\beta^{PH}$ into the cellular acidic organelles, thereby avoiding detection of peptide sticking to the cell surface. $A\beta^{PH}$ fluorescence after phagocytosis is sufficiently bright to enable FACS experiments, allowing single cell analysis of $A\beta^{PH+}$ phagocytic and $A\beta^{PH-}$ non-phagocytic microglia and other glial cells.

Fixing cells that have internalized $A\beta^{PH}$, and using specific antibodies and dyes to study specific molecular processes, can help identify molecular mechanisms involved during $A\beta$ phagocytosis. To determine whether $A\beta^{PH}$ can maintain its fluorescence in fixed cells, we used primary mouse CD11b$^+$ microglial cells isolated from 3–5 month old mice as well as BV2, N9, and HMC3 microglia. After $A\beta^{PH}$ (5.0 μM) treatment for 2 hours, the cells were fixed in 4% paraformaldehyde followed by addition of red phalloidin dye (a podosome core marker for F-actin) to visualize actin filaments and the cell body with confocal microscopy (Fig. S14A and B†). Confocal imaging of the fixed $A\beta^{PH}$-treated microglia showed green fluorescence within the red actin filaments thereby confirming the uptake of $A\beta^{PH}$ peptides by the cells. Further, LysoTracker DND-99 was used to confirm localization of $A\beta^{PH}$ within acidic organelles such as phagosomes or phagolysosomes. The co-localization of green fluorescent $A\beta^{PH}$ along with the red signal from the LysoTracker dye confirmed the presence of $A\beta^{PH}$ within acidic phagolysosomes after 2 hours in HMC3, N9, and BV2 microglial cell lines (Fig. 2A and S14C†). Similarly, uptake of $A\beta^{PH}$ into intracellular acidic organelles was also confirmed in CD11b$^+$ primary microglia that were cultured in reduced-serum TIC medium[40] (Fig. 2B). Finally, we also detected the green fluorescence signal within CD11b$^+$ primary microglia ($A\beta^{PH+}$ cells) at 0.5, 1.0, and 2.0 μM $A\beta^{PH}$ concentrations *via* flow cytometry (Fig. 2C and S13B†) after 1 hour of treatment, and found an increase in fluorescence with $A\beta^{PH}$ concentration. The unstained and live/dead stained cells were used as controls.

Microglia recognize and phagocytose $A\beta$ peptides through scavenger receptors such as Toll-Like Receptor 2 (TLR2), Cluster of Differentiation 14 (CD14), and Triggering Receptors Expressed on Myeloid Cells 2 (TREM2).[41–43] Studies have shown that deletion of, or mutations in $A\beta$-specific receptors, such as TREM2, leads to increased $A\beta$ seeding.[44,45] Thus, the $A\beta^{PH}$ reporter that we have developed could serve as a valuable chemical tool to delineate the role of receptor proteins involved in $A\beta$ uptake by glial cells, using specific antibodies or CRISPR-Cas9 genetic screens.

In addition to microglia, astrocytes have been shown to exhibit phagocytic characteristics after ischemic injury[16] and can phagocytose extracellular $A\beta$.[28] Therefore, we tested whether primary immunopanned cultured rat astrocytes phagocytosed $A\beta^{PH}$. Indeed, this was the case, with retention of the phagocytic $A\beta^{PH}$ signal after methanol-fixation and staining of cells with GFAP antibody (Fig. 2D). $A\beta^{PH}$ phagocytosis could also be detected with live cell imaging (Fig. 2E). Quantification of $A\beta^{PH}$ uptake at different concentrations showed internalization increasing for approximately 1 hour, followed by a sustained fluorescence within the cells which may reflect a balance between phagocytosis and degradation of the probe (Fig. 2F). Thus, $A\beta^{PH}$ may be a viable candidate for concentration- and time-dependent studies of glial cell phagocytosis *in vitro*. The sustained fluorescence of $A\beta^{PH}$ seen for up to 6 hours inside cultured microglia and astrocytes suggests that it is chemically stable under physiological conditions – allowing for long-term use *in vivo*.

$A\beta^{PH}$ uptake by microglia and astrocytes in hippocampus, cortex, and retina

To assess phagocytic uptake of $A\beta^{PH}$ in the hippocampus, a brain area that is crucial for learning and memory, we applied 5 μM $A\beta^{PH}$ (for 1.5 hours at 37 °C) to live hippocampal slices from postnatal day 12 (P12) rats. The tissue slices were then fixed and stained with glial cell specific antibodies (Fig. 3A). Microglia phagocytosed $A\beta^{PH}$ as seen by the localization of $A\beta^{PH}$ within the IBA1$^+$ myeloid cells in these tissues (Fig. 3B). Our experiments revealed green fluorescent signal both within IBA1$^+$ microglial cells as well as outside the IBA1$^+$ cells (Fig. S15†), presumably reflecting phagocytic uptake of $A\beta^{PH}$ by cells other than microglia, such as astrocytes. Indeed, staining with GFAP antibody demonstrated internalization of $A\beta^{PH}$ within GFAP$^+$ astrocytes (Fig. 3C). Summing over cells, approximately 60% of the internalized $A\beta^{PH}$ was phagocytosed by microglia and 40% by astrocytes (Fig. 3D). Interestingly, in astrocytes the phagocytosed $A\beta^{PH}$ was distributed more homogeneously throughout the GFAP area than the phagocytosed $A\beta^{PH}$ in IBA1 stained microglia. This is expected since in microglia the acidic compartments (where $A\beta^{PH}$ is present) are mostly juxtanuclear whereas IBA1 is known to be enriched in podosomes and podonuts.[46] In contrast, in astrocytes the acidic compartments occur all over the cell body.[47]

We next tested the $A\beta^{PH}$ probe in different *in vivo* settings. After intracranial injection of $A\beta^{PH}$ into the somatosensory cortex of wild-type P7 C57BL/6J mice (Fig. 4A), phagocytosis of
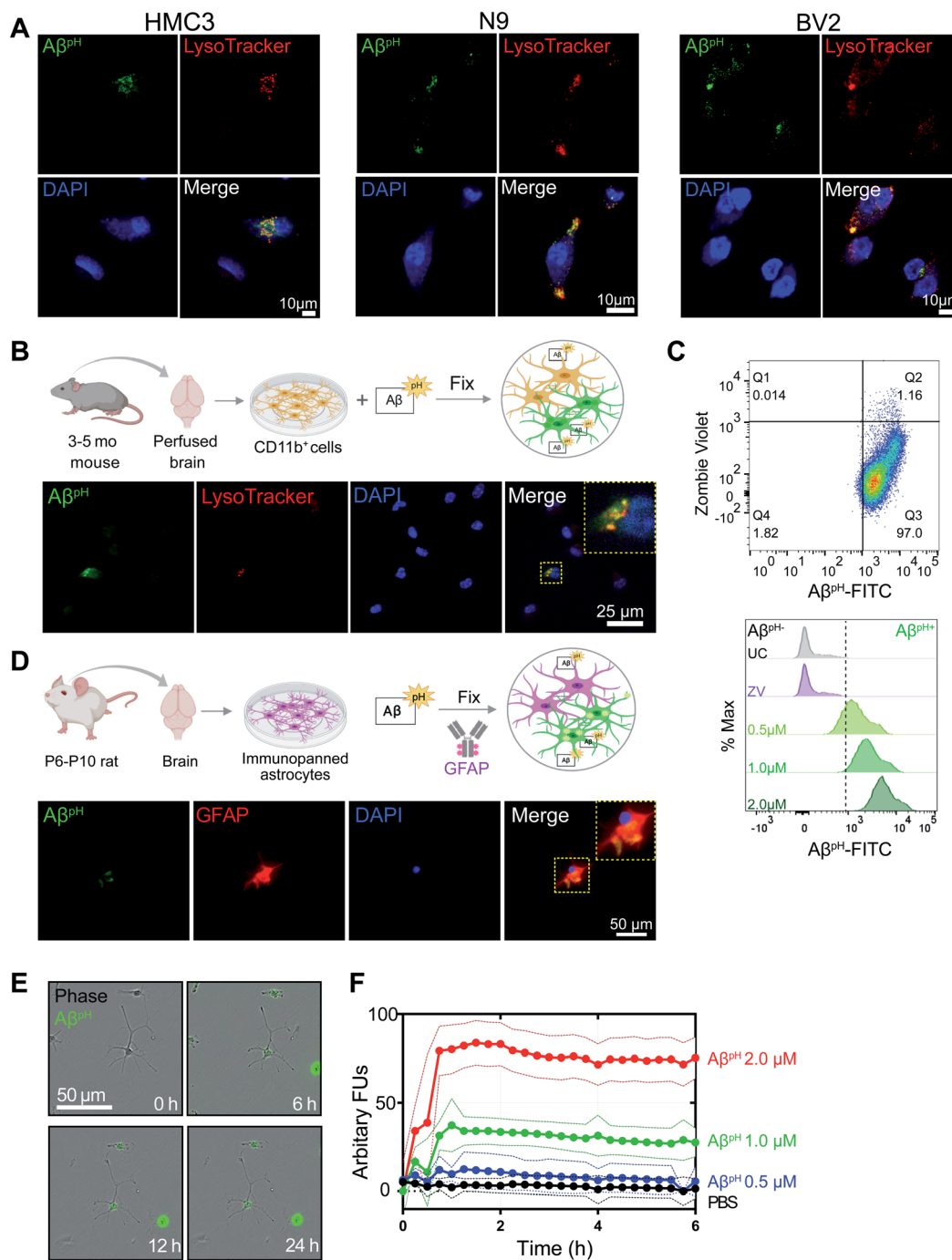
Fig. 2 Fluorescence of internalized $A\beta^{pH}$ is retained in fixed cells. (A) Confocal images of fixed HMC3, N9, and BV2 cells showing the uptake of $A\beta^{pH}$ (green). Cells are stained for acidic intracellular organelles (LysoTracker Red, confirming co-localization of the $A\beta^{pH}$ within the acidic intracellular organelles) and nuclei (DAPI, blue). No antibody is required to detect $A\beta^{pH}$. (B) Primary mouse microglia grown in defined, reduced-serum media phagocytose $A\beta^{pH}$ *ex vivo*. Cells are fixed and stained for nuclei and show $A\beta^{pH}$ colocalized in the acidic organelles with LysoTracker Red. (C) The phagocytic uptake of $A\beta^{pH}$ by primary microglia is measured and quantified *via* flow cytometry analysis. Dot plot shows live (ZV$^-$) and $A\beta^{pH+}$ cells. No green fluorescence is measured in unstained cells (UC) or dead cells stained with the ZV live/dead stain only whereas green fluorescence is measured in cells treated with 0.5, 1.0, and 2.0 μM $A\beta^{pH}$ for 1 hour. Data shown in terms of % max, by scaling each curve to mode = 100% (*y*-axis). (D) Primary immunopanned rat astrocytes also phagocytose $A\beta^{pH}$ in serum-free conditions. Cells are fixed and stained for astrocyte specific GFAP antibody (red) and nuclei. (E) Uptake of $A\beta^{pH}$ over time by primary immunopanned astrocytes as observed in live cells in real time. (F) Quantification of uptake of 0.5, 1.0, and 2.0 μM $A\beta^{pH}$ by primary astrocytes. Data are mean ± SEM, $n = 8$ separate wells per group/timepoint.

the $A\beta^{pH}$ by IBA1$^+$ microglia and GFAP$^+$ astrocytes was assessed by fixing the corresponding tissue sections at 24 and 72 hours after injection. At 24 hours, $A\beta^{pH}$ was observed in the injected area and appeared to be enclosed within cell bodies. There was less astrocyte uptake of $A\beta^{pH}$ compared to uptake by microglia, which may be a result of a reactive response by astrocytes that
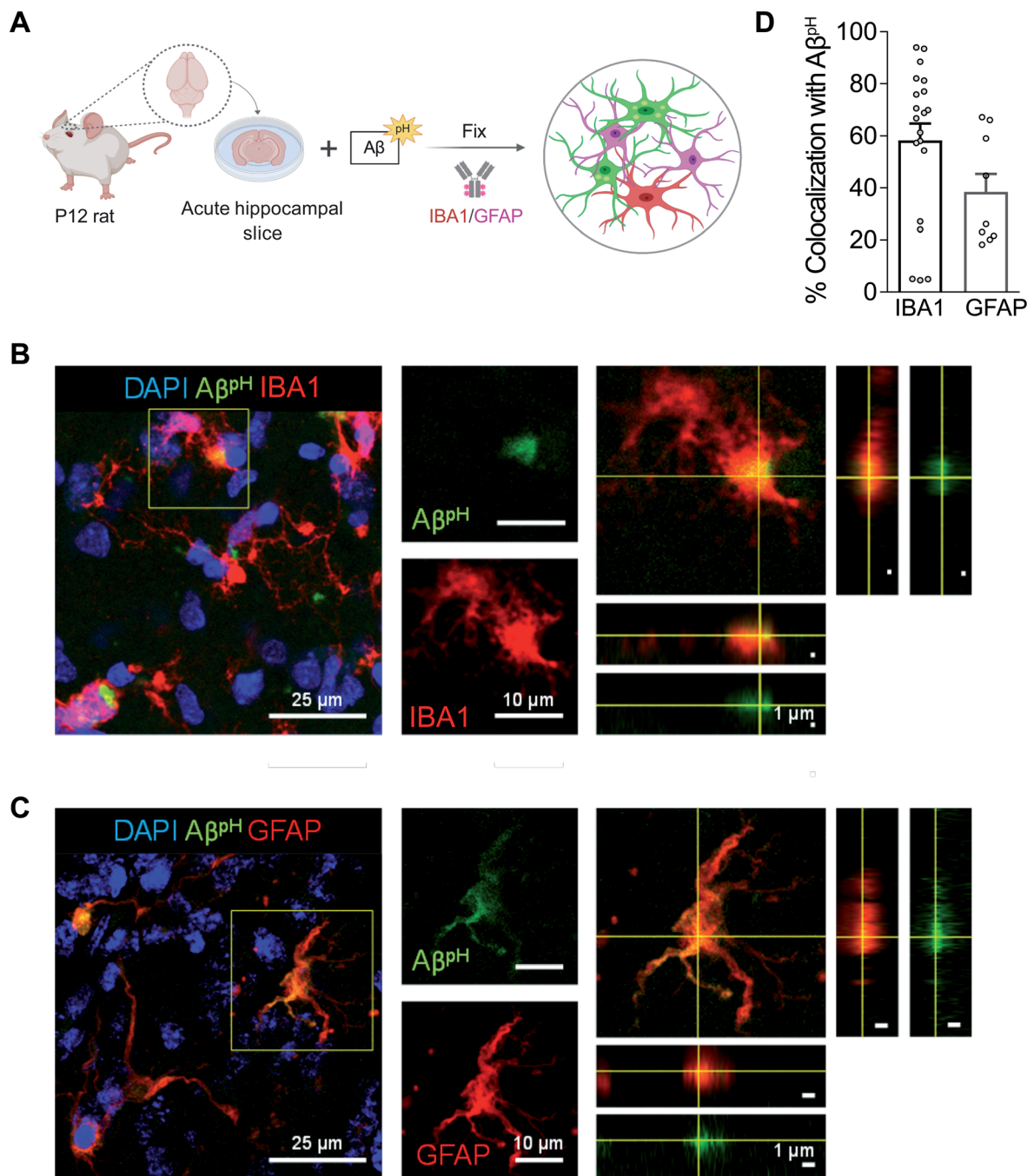
Fig. 3 AβpH is phagocytosed by both microglia and astrocytes *in situ* in rat hippocampal tissue sections. (A) Schematic of phagocytosis assay in rat hippocampal tissue slices. (B) Representative 2D maximum projection of a confocal z-stack showing microglia phagocytosing AβpH. Closeup of the indicated cell (yellow square) is shown on the right. Orthogonal projections at the level of the crosshairs show internalization of AβpH within the microglia. (C) Representative 2D maximum projection of a confocal z-stack showing astrocytes phagocytosing AβpH. Closeup of the indicated cell (yellow square) is shown on the right. Orthogonal projections at the level of the crosshairs show internalization of AβpH within the astrocyte. (D) Quantification of AβpH colocalized with microglia and astrocytes, as defined by IBA1⁺ and GFAP⁺ staining, respectively. Data shown as mean ± s.e.m. collected from 20 and 8 slices for microglia and astrocytes respectively (from 3 animals).

has been shown to downregulate phagocytic pathways in some states[5] (Fig. 4B and D). At 72 hours after the AβpH injection there was also AβpH visible at the pial surface and in the periventricular white matter. With increased magnification, we observed cell bodies containing AβpH that were positive for the IBA1 microglial marker (Fig. 4C) but the GFAP⁺ astrocytes

localized at the injection site showed very little AβpH signal (Fig. 4D). Thus, microglia engulf the majority of the AβpH under these conditions *in vivo* with astrocytes also contributing to removal at early times.

Next, we injected AβpH into the vitreous of the eye in postnatal rats to eliminate possible complications due to glial
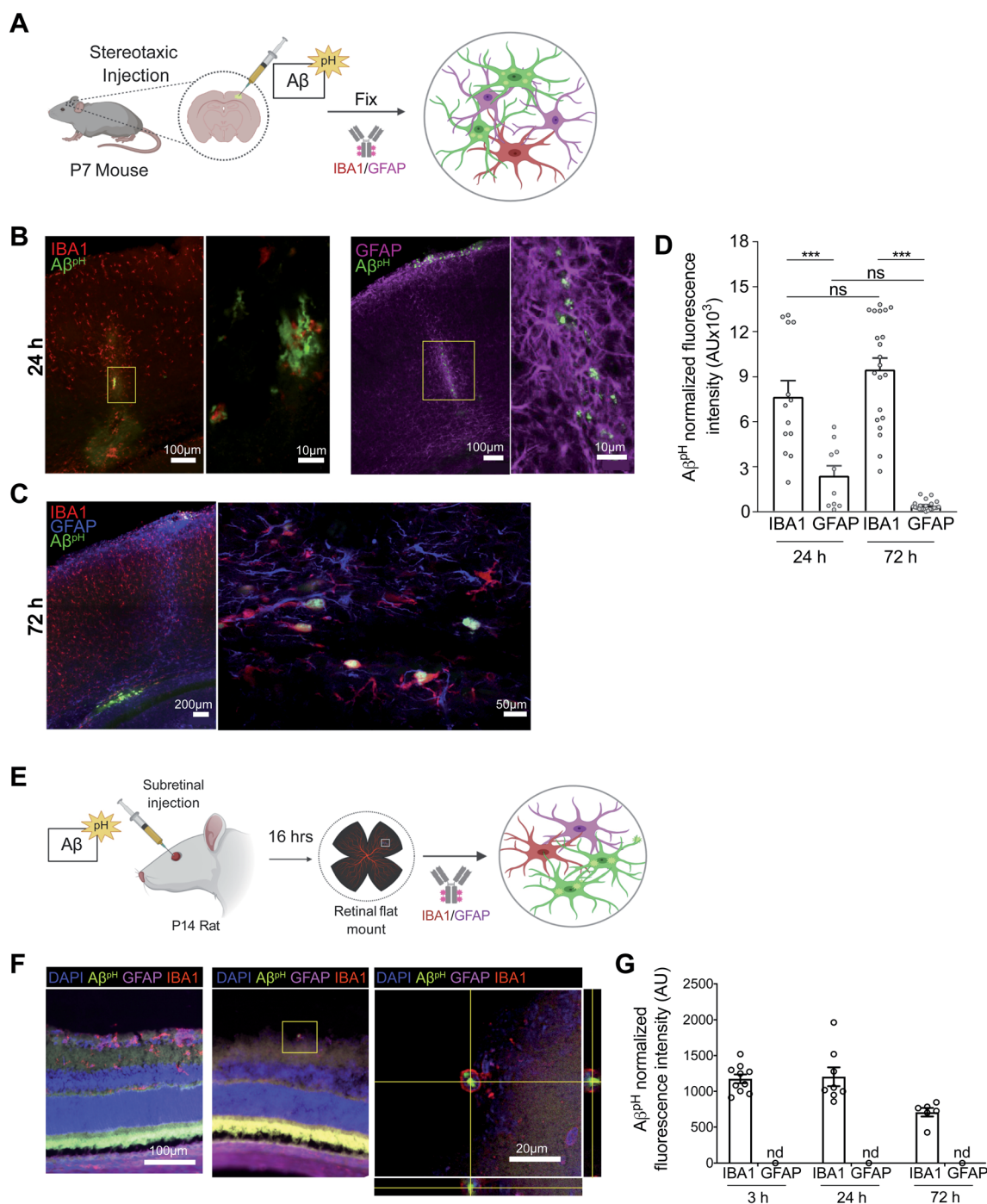
Fig. 4 Aβ^{pH} is phagocytosed by cortical microglia and astrocytes *in vivo* and by rat retinal microglia *in vivo*. (A) Schematic of stereotaxic microinjection of Aβ^{pH} in the somatosensory cortex of P7 mouse followed by staining of fixed tissue section after 24 and 72 hours. (B) Phagocytic uptake of Aβ^{pH} by IBA1^{+} microglia and GFAP^{+} astrocytes in the periventricular white matter at the 24 hour timepoint. The box represents the region of the fluorescence image where high magnification confocal imaging was done. (C) IBA1^{+} microglia show bright green fluorescence at 72 hours in the same region indicating presence of Aβ^{pH} within the cells at this timepoint. GFAP^{+} astrocytes do not show any green fluorescence in this region at this timepoint suggesting either degradation of the peptide or insufficient Aβ^{pH} concentration for detectable phagocytic uptake by these cells. (D) Quantification of Aβ^{pH} fluorescence within IBA1^{+} microglia and GFAP^{+} astrocytes located in the pia and white matter regions show more Aβ^{pH} uptake by microglia compared to astrocytes. (E) Schematic of subretinal injection of Aβ^{pH} to evaluate its *in vivo* uptake by rat retinal microglia and astrocytes. (F) IBA1^{+} rat retinal microglia phagocytose Aβ^{pH} *in vivo*. (G) Quantification of Aβ^{pH} uptake into retinal IBA1^{+} microglia and GFAP^{+} astrocytes. No fluorescence was detected in astrocytes at these 3 time points (n.d.). Data shown as mean ± s.e.m. from 2 animals.

scarring resulting from cortical injection, and low penetration through the blood–brain barrier as a result of peripheral delivery (Fig. 4E). We injected 1 μL of Aβ^{pH} intravitreally and left the animals for 3, 24, or 72 hours. At the end of the experiment, retinae were removed, fixed in 4% paraformaldehyde, and whole mount retinal preparations were made. Astrocytes and microglia in the retinal ganglion cell layer were labelled with GFAP and IBA1 antibodies respectively, and co-localization with
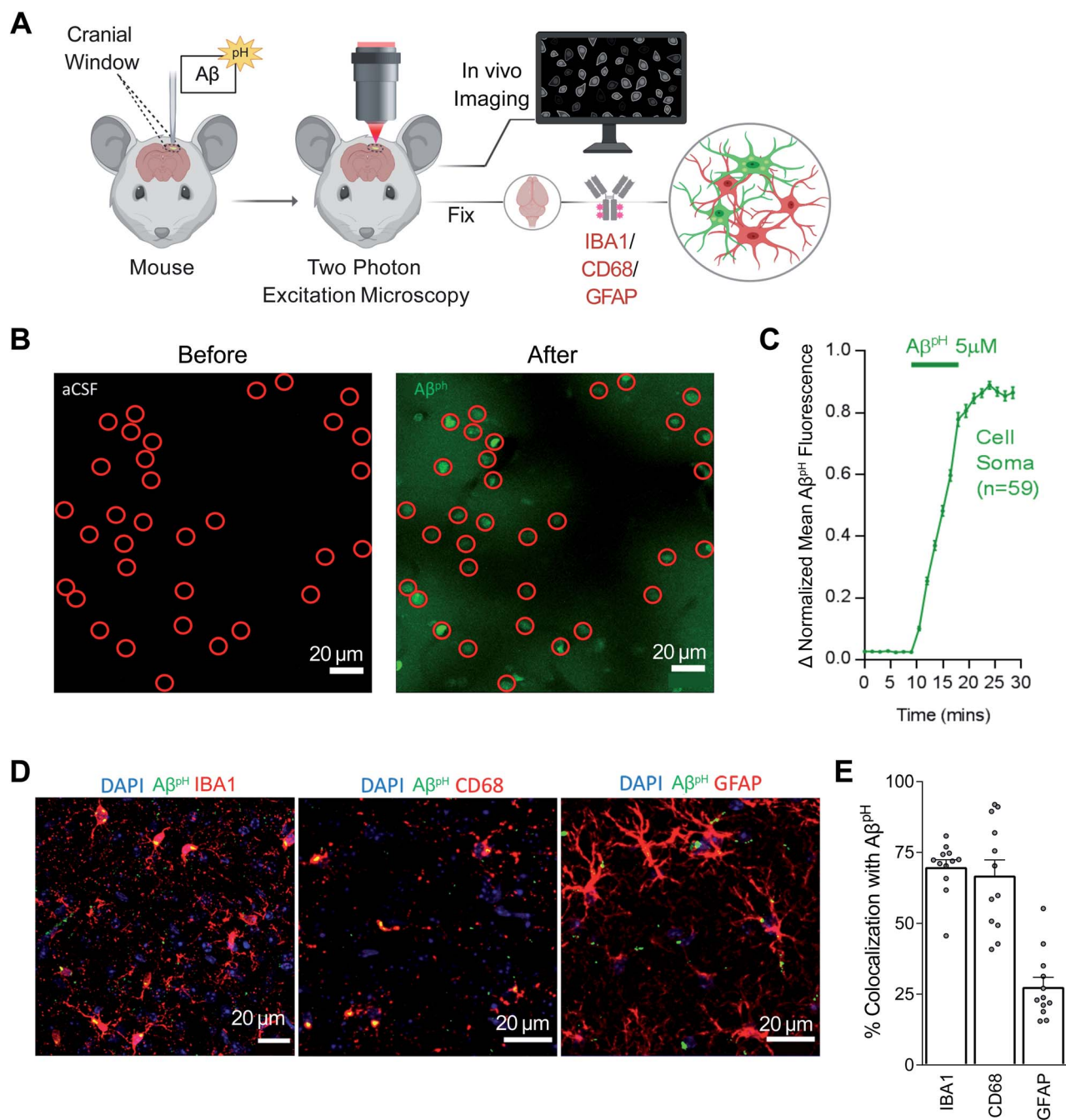

Fig. 5 Aβ^{pH} is phagocytosed by microglia and astrocytes *in vivo* in the cerebral cortex. (A) Schematic of how Aβ^{pH} phagocytic uptake is imaged through a cranial window *in vivo* in real time using two-photon excitation microscopy. (B) *In vivo* two-photon imaging of the mouse barrel cortex before and after topical application of Aβ^{pH}. The fluorescence increases in cell somata (indicated by red circles) reflecting Aβ^{pH} uptake. Shadows in the right image are created by the presence of pial and intraparenchymal vessels. (C) Quantification of mean Aβ^{pH} fluorescence in cell somata over time. The data were normalized to the maximum mean Aβ^{pH} fluorescence for each cell and then averaged. Data shown as mean ± s.e.m. N = 59 somata from 2 animals. (D) 1.5 to 3 hours after *in vivo* two-photon imaging of Aβ^{pH}, animals were perfusion-fixed and cortical slices were stained for microglia, lysosomes/endosomes, and astrocytes using IBA1, CD68, and GFAP antibodies, respectively. (E) Quantification of Aβ^{pH} colocalization with IBA1, CD68, and GFAP suggests that most Aβ^{pH} is taken up by microglia and astrocytes *in vivo*. Data shown as mean ± s.e.m. N = 12 stacks from 3 animals.

the fluorescent signal from the injected Aβ[PH] probe was determined. We observed that IBA1^{+} microglia contained Aβ[PH] at all time points, but we did not detect any Aβ[PH] signal in GFAP[+] astrocytes (Fig. 4F and G). The Aβ[PH] positive microglia were less visible in the retina compared to other brain regions, suggesting that clearance from the eye was more rapid than clearance from the brain parenchyma as observed in other experiments (above).

The in vivo investigation of Aβ phagocytosis described above consists of imaging fixed tissue sections with confocal microscopy. To date, phagocytosis of Aβ has not been observed in live animals in real time. Using Aβ[PH], we observed phagocytic uptake in live mice in real time using two-photon microscopy (Movies S4 and S5†). Here, 5.0 μM Aβ[PH] was applied onto the cortical surface of live mice through a cranial window for 10 minutes during two-photon imaging of the barrel cortex (Fig. 5A). This showed an increase in green fluorescence in the cell somata after Aβ[PH] application, indicating phagocytic uptake of Aβ[PH] (Fig. 5B). Quantification of the fluorescence within the cell somata showed rapid Aβ[PH] uptake after the peptide was added to the cranial window followed by stabilization of the signal at around 20 minutes (Fig. 5C). The brains were later fixed by cardiac paraformaldehyde perfusion and stained with antibodies to identify the cell types mediating the Aβ[PH] uptake. Phagocytosed green Aβ[PH] was present in IBA1 labeled microglia and colocalized with the microglial/macrophage lysosomal protein CD68, and Aβ[PH] was also seen in GFAP[+] astrocytes (Fig. 5D). Integrating the fluorescence over the different classes of labeled cells showed that about 70% of the phagocytosed Aβ[PH] was taken up by microglia and about 25% by astrocytes (Fig. 5E). These percentages are similar to those seen in the brain slice experiments described above. Thus, microglial uptake of Aβ[PH] dominates over astrocyte uptake.

Discussion

The phagocytic capacity of glial cells has been measured using traditional dyes and fluorophore-labeled particles such as fluorescein or rhodamine-coated E. coli and beads, however, these experiments entail some major drawbacks: (1) difficulty in differentiating between adherent versus internalized particles, (2) use of additional reagents (like trypan blue or ethidium bromide) and additional experimental steps required to quench the extracellular fluorescence prior to analysis by flow cytometry and imaging,[48] (3) quenching of the fluorescence within the acidic environment of the phagosomes, and (4) lack of specificity of the neuronal target substrate (beads, E. coli, zymosan, etc.).[49] Here, we have synthesized a pH-sensitive fluorogenic Aβ reporter, Aβ[PH], at a microgram scale and characterized the reporter in detail (Fig. 1A–C and S2–S11†). We show that the Aβ[PH] is well suited for detection in the acidic environment of the lysosomal organelles with pH of 5.0–4.5. The PTXG dye has an acidic pK_a of 4.4–4.7 in DMEM/F12 cell culture medium and exhibits a gain of fluorescence in the acidic environments. Upon conjugation with Aβ, the pK_a of Aβ[PH] probe shifts to 5.2–5.9, which is in the range of acidic lysosomal organelles and is thus ideal for future mechanistic studies. Moreover, the unconjugated PTXG dye exhibits low to no background fluorescence

signal, compared to other commercial dyes such as pHrodo-Red SE, justifying its in vitro and in vivo use. We demonstrated the functionality of Aβ[PH] in mouse and human microglial cell lines, in primary microglial and astrocyte cultures in vitro, in acute hippocampal slices from mouse brains, in mice in vivo using stereotaxic injections followed by fixation, and in live mice in vivo via two-photon imaging. The Aβ[PH] reporter is a powerful tool for answering questions related to mechanisms of Aβ phagocytosis and cellular inflammatory responses, and for developing therapeutic strategies to promote Aβ clearance.

We observed phagocytic uptake of Aβ[PH] in three different microglial cell lines and in primary glial cell cultures in real-time (Fig. 1D, E, 2E and F) and by using confocal imaging (Fig. 2A, B and D). We showed the utility of Aβ[PH] to be used without the need for any antibodies to identify or detect Aβ using flow cytometry (Fig. 1F and 2C) which will greatly benefit experimental design and outcome by reducing the number of steps required in assays. While microglia cultured in vitro and ex vivo do not completely recapitulate the transcriptomes of microglia in vivo,[50] microglial cell culture models provide a convenient system for screening chemical and biological molecules in a rapid and high-throughput manner. We also demonstrated the utility of Aβ[PH] in functional assays to evaluate cellular phagocytosis. Further, we demonstrated the phagocytic uptake of Aβ[PH] in live tissue hippocampal slices that preserve the three-dimensional nature of the cell microenvironment and can serve as an additional useful model to study Aβ-related biology in a tissue environment. Microglia were more efficient in internalizing Aβ[PH] than astrocytes in situ (Fig. 3A–D). During the period of this assay it is unlikely that astrocytes would have become reactive so it appears that Aβ clearance is not just a property of reactive astrocytes.[51–53] The astrocytes most closely associated with neurodegeneration appear to be of a reactive phenotype that downregulates phagocytic pathways,[5] suggesting that the engulfment of Aβ[PH] by astrocytes is a normal physiological function of these cells (although this may change with disease progression).

Most importantly, we demonstrated the utility of using of Aβ[PH] in various in vivo models. Stereotaxic injection of Aβ[PH] into the mouse somatosensory cortex was followed by uptake by microglia and astrocytes (Fig. 4A–D), injecting Aβ[PH] into the vitreous of the eye was followed by uptake by retinal microglia (Fig. 4E–G), and the real-time uptake of Aβ[PH] by microglia and astrocytes was demonstrated in vivo in live mice using two-photon microscopy (Fig. 5A–C). We confirmed the identity of the cells observed with two-photon excitation by using IBA1 to label microglia, CD68 (a phagocytosis-specific marker) to label microglia and macrophages, and GFAP to label astrocytes (Fig. 5D and E). The time course of uptake in vivo was rapid, with phagocytosed Aβ[PH] fluorescence reaching a peak level within 20 minutes (this may reflect a balance between continued phagocytosis and intracellular degradation). Approximately two thirds of the Aβ[PH] was phagocytosed by microglia and one third by astrocytes, again on a time scale too rapid for astrocytes to have become reactive.

The development of Aβ[PH], in particular the ease with which it can be produced in the lab, will facilitate the characterization of

different populations of cells that remove (or do not remove) Aβ by phagocytosis in various conditions, including AD, trauma-induced amyloidopathy and Down's syndrome. Combining this tracer with transgenic labeling of microglia (e.g. Tmem119-tdTomato mice[54] which exhibit red fluorescence in microglia) or other cell types will allow the transcriptome and proteome of different subpopulations of heterogeneous phagocytic cells to be defined (including cells of different age,[25,55,56] and sex[57]), facilitating the discovery of new mechanisms, targets and functional biomarkers. Understanding the clearance of Aβ is fundamental to understanding the onset of AD,[58,59] and having a quantitative technique to assess Aβ phagocytosis should contribute significantly to this. We expect that AβpH will become a useful tool to facilitate the study of impaired phagocytic function mechanisms in vivo during chronic inflammation in neurodegenerative diseases.

Material and methods

Animal ethics

Animal maintenance and isolation of primary microglia were performed according to Purdue Animal Care and Use Committee guidelines and approval (protocol number 1812001834). Injection of AβpH into the retina of rats were completed in accordance with the National Institute of Health Stanford University's Administrative Panel on Laboratory Animal Care. Purification of rat primary astrocyte was completed in accordance with NYU Langone School of Medicine's Institutional Animal Care and Use Committee (IACUC) guidelines and approval. All rats were housed with ad libitum food and water in a 12 hour light/dark cycle. Standard Sprague Dawley rats (Charles River, #400) were used in all retinal experiments. Animal maintenance and experimental procedure for the intracranial stereotaxic injections of AβpH in mice were performed according to the guidelines established by the IACUC at Harvard Medical School (protocol number IS00001269). Experiments on brain slices and in vivo 2-photon imaged mice were carried out under a UK government license (PPL 70/8976, awarded after local ethical review and UK Home Office assessment) to David Attwell, in accordance with all relevant animal legislation in the UK.

Synthesis of pH-sensitive fluorescent human Aβ conjugate with Protonex Green™ (AβpH)

Human amyloid-beta (Aβ$_{1-42}$) was purchased from AnaSpec., Inc (Cat. #AS-20276, extinction coefficient at 280 nm based on single tyrosine residue is 1490 M^{-1} cm^{-1}), Protonex™ Green 500 SE was from AAT Bioquest, Inc. (Cat. #21215, absorbance maximum 457 nm, extinction coefficient 4000 cm^{-1} M^{-1}, correction factor at 280 nm 1.069). To 200 μL aliquot of monomeric Aβ$_{1-42}$ (1 mg mL^{-1} in 1 M NaHCO$_3$, pH ~8.3) was added 10 equivalents of Protonex-Green 500 (PTXG), SE dye (88 μL from 5 mM stock in anhydrous DMSO) and incubated at room temperature for 3 hours in the dark (vial wrapped in aluminum foil: note: add 100 μL ultrapure water if the solution becomes viscous). The additional 5 equivalents of PTXG, SE dye

(44 μL from 5 mM DMSO stock) was added and incubated under the same conditions for 3 hours. The crude reaction mixture was diluted with 1 mL ultrapure water and the conjugated product was dialyzed by Pierce Protein Concentrators at 4500 g for 30–45 minutes in a swinging bucket centrifuge to remove the small molecular weight fragments [Pierce Protein Concentrators PES, 3K Molecular Weight Cut-Off (MWCO); Thermo Fisher Scientific, Cat #PI88514, note: prior use, wash and centrifuge protein concentrator with 1 mL ultrapure water to remove any preservatives]. The resulting concentrated solution was diluted with 0.5 mL ultrapure water and dialyzed again for 15–30 minutes as done previously. Then the concentrated solution was diluted with 0.2 mL ultrapure water and lyophilized overnight to get the AβpH powder. Protein or dye concentration can be calculated using parameters mentioned above. Finally, MALDI-MS spectrum was recorded to confirm the chemical conjugation of PTXG with Aβ$_{1-42}$.

Synthesis of pH-sensitive fluorescent human Aβ$_{1-42}$ conjugate with pHrodo (RODO–AβpH)

The pHrodo-Red SE was purchased from Thermo Fisher Scientific (Cat. #P36600, absorbance maximum 560 nm, extinction coefficient 65 000 M^{-1} cm^{-1}, correction factor at 280 nm 0.12). A solution containing monomeric Aβ$_{1-42}$ (570 μg, 12.63 nmol) was prepared in 1 M NaHCO$_3$ (pH 8.3, 570 μL) and the pHrodo Red-NHS (1 mg) stock solution was prepared in anhydrous DMSO (150 μL) (~10.2 mM). Next, the Aβ solution (570 μL) and pHrodo stock solution (0.6314 μmol, 61.5 μL of stock solution) were mixed and incubated at room temperature for 6 hours while wrapped with aluminum foil. This crude reaction mixture was then diluted with ultrapure water (1 mL) and the conjugated product was dialyzed by Pierce Protein Concentrators (PES, 3K MWCO, note: prior use, wash and centrifuge protein concentrator with 1 mL ultrapure water to remove any preservatives) at 4500 g for 30–45 minutes in a swinging bucket centrifuge to remove the small molecular weight fragments. The resulting concentrated solution was diluted with ultrapure water (0.5 mL) and dialyzed again for 15–30 minutes as before. Then the concentrated solution was diluted with 0.2 mL ultrapure water and lyophilized overnight to get the RODO–AβpH powder. Protein or dye concentration can be calculated using parameters mentioned above. Finally, the MALDI-MS spectrum was recorded to confirm the chemical conjugation of pHrodo-Red fluorophore to the Aβ peptide.

Preparation of HFIP-treated Aβ and AβpH stocks

Aβ or AβpH was dissolved in HFIP and prepared as previously described.[37] Briefly, 1 mM Aβ solution was prepared by adding HFIP directly to the vial (0.5 mg Aβ or AβpH in 93.35 μL HFIP). The peptide should be completely dissolved. The solution was incubated at room temperature for at least 30 min. HFIP was allowed to evaporate in the open tubes overnight in the fume hood and then dried down under high vacuum for 1 hour without heating to remove any remaining traces of HFIP and moisture, leaving a thin clear film of peptide at the bottom of the tubes. The tubes containing dried peptides were stored at

−20 °C until further use. To make oligomers, 5 mM Aβ DMSO stock was prepared by adding 22 μL fresh dry DMSO to 0.5 mg of dried peptide film. To ensure complete resuspension of peptide film, the mixture was pipetted thoroughly, scraping down the sides of the tube near the bottom. The suspension was vortexed well (~30 seconds) and pulsed in a microcentrifuge to collect the solution at the bottom of the tube and the 5 mM Aβ DMSO solution was sonicated for 10 minutes. This preparation was used as the starting material for preparing the aggregated Aβ incubated at 4 °C for 24 hours for analysis by atomic force microscopy.

Atomic force microscopy for analysis of Aβ and Aβ^{PH} aggregates

We followed the previously published detailed protocols for analyzing Aβ and Aβ^{PH} aggregates by atomic force microscopy (AFM).[37,38] Briefly, sample preparation was performed with sterile techniques using sterile media and MilliQ-water. A 10 mL syringe with ultrapure water equipped with a 0.22 μm filter was filled and the initial 1–2 mL was discarded though syringe filter output. 1 M HCl and 1× PBS buffer were also filtered through 0.22 μm filter. The samples were prepared for spotting on mica by diluting to final concentrations of 10–30 μM in water. Immediately before sample delivery, top few layers of mica were cleaved away using an adhesive tape to reveal a clean, flat, featureless surface. The fresh surface was pretreated with ~5–8 μL of filtered 1 M HCl for 30 seconds and rinsed with two drops of water (note: the mica was held at a 45° angle and washed with water to allow the water coming out of the syringe filter to roll over the mica). If necessary, the remaining water was absorbed with fiber-free tissue paper/wipes by keeping paper on the edge of the mica. Immediately, the sample was spotted onto mica and incubated for 3 minutes followed by rinsing with three drops of water and blow drying with several gentle pulses of compressed air. Samples were then kept in a dust-free box and incubated on benchtop for a few minutes to hours at room temperature until analysis. AFM imaging was performed with Veeco Multimode with NanoScope V controller with NanoScope Software using the Silicon AFM probes, TAP300 Aluminum reflex coating (Ted Pella, Inc. Cat# TAP300AL-G-10) at ~300 kHz resonant frequency and ~40 N m^{-1} force constant in the tapping mode.

pH-dependent emission spectra of Aβ conjugated with Protonex Green® and Aβ conjugated with pHrodo at various concentrations

The cell culture medium was supplemented with dilute HCl and NaOH solutions to obtain different solutions of pH ranging from 1.0 to 9.0 for the assay. Lyophilized powder of Aβ conjugated with pHrodo (RODO–Aβ^{PH}) and Aβ conjugated with Protonex Green® (PTXG–Aβ^{PH}) was dissolved in cell culture medium to make stock solutions and kept at 37 °C for 24 hours to pre-aggregate the peptide conjugates. From the stock solutions, different dilutions for each pH condition were prepared at concentrations of 0.5, 1.0, 2.0, and 5.0 μM in a 96-well plate (100 μL per well). Fluorescence intensity of each well containing

Aβ^{PH} was obtained on a Cytation™ 5 imaging multi-mode reader (BioTek Instruments) at 443/505 nm excitation/emission wavelengths. The fluorescence intensity of each pH-solution and Aβ^{PH}-concentration in relative fluorescence units (RFU) was plotted using GraphPad Prism software.

pK_a of Protonex Green 500, SE® (PTXG), Aβ^{PH}, and RODO–Aβ^{PH}

The cell culture medium DMEM/F12 (Corning Cat.# MT15090CV) was supplemented with dilute HCl and NaOH solutions to obtain different pH solutions (pH range 3.85, 4.03, 4.26, 4.46, 4.88, 5.02, 5.30, 5.67, 6.22, 6.44, 6.94, 7.40, 8.31) for the assay. From the stock solutions (5 mM of PTXG and 100 μM of Aβ^{PH}) different dilutions for each pH condition were prepared at concentrations of 5.0, 2.0, 1.0, 0.5 μM in a 384-well plate with 40 μL per well total volume (Corning NBS plate, cat #3575). Fluorescence intensity of each well containing PTXG and Aβ^{PH} was obtained on a Varioskan LUX imaging multi-mode reader (Thermo Scientific) at excitation/emission wavelengths 443/505 nm for PTXG or Aβ^{PH} and excitation/emission wavelengths 466/590 nm for RODO–Aβ^{PH}. The fluorescence intensity was normalized by diving each value by the highest value obtained for 5 μM concentration. The fluorescence intensity of each pH-solution vs. Normalized fluorescence intensity for each concentration was plotted using three replicates and processed using GraphPad Prism software.

Concentration-dependent response of Protonex Green 500, SE® and Aβ^{PH} at acidic pH over time

Solutions of Protonex Green 500, SE® (PTXG) and Aβ conjugated with PTXG (Aβ^{PH}) were prepared in the cell culture medium at concentrations of 0, 0.1, 0.5, 1.0, 2.0, 5.0 μM and a 50 μL aliquot of each solution was transferred in duplicates into the wells of a 96-well plate. To measure the florescence of PTXG and Aβ^{PH} solutions under acidic conditions at different concentrations, 7.5 μL of pH 1.0 solution (hydrochloric acid in media) was added to each well to obtain a final pH of 3.0. Fluorescence intensities of the acidic solutions were measured at an excitation/emission wavelength of 443/505 nm on A Cytation 5 multimode plate reader (BioTek, Inc). Next, to initiate aggregation of Aβ^{PH}, the plate was incubated at 37 °C with 5% CO$_2$ and fluorescence was measured at 2, 6, 12, and 24 hour time points. The change in fluorescence intensities of the PTXG and Aβ^{PH} aggregates was analyzed over time using GraphPad Prism software.

Cell lines – culture and maintenance

BV2 and N9 mouse microglial cell lines were generously gifted by Dr Linda J. Van Eldik (University of Kentucky, USA). The BV-2 cell line was developed in the lab of Dr Elisabetta Blasi at the University of Perugia, Italy. Cells were maintained at 37 °C and 5% CO$_2$ in DMEM (Dulbecco's Modified Eagle's Medium)/Hams F-12 50/50 Mix (Corning #10-090-CV) supplemented with 10% FBS (Atlanta BiologiBiologics), 1% L-glutamine (Corning #25-005-CI), and 1% penicillin/streptomycin (Invitrogen). HMC3 human microglial cell line was a gift from Dr Jianming Li

(Purdue University, USA) who originally obtained the cells from ATCC. These cells were maintained at 37 °C and 5% CO_2 in DMEM supplemented with 10% FBS and 1% penicillin/streptomycin.

Background fluorescence of PTXG and RODO in cells

BV2 cells were seeded at a concentration of 10 000 cells in 200 μL per well in a 96-well flat-bottom plate (Falcon) for 16 hours (overnight). The next day, the media was aspirated, and the cells were treated with 1.0 μM or 0.5 μM of PTXG, PTXG–Aβ^{PH}, RODO, and RODO–Aβ^{PH} and placed in a 37 °C incubator for 2 hours respectively. Next, the fluorescence of PTXG and PTXG–Aβ^{PH} was measured at 443/505 nm and the fluorescence of RODO, and RODO–Aβ^{PH} was measured at 560/585 nm using a fluorescence plate reader (Attune NxT, Thermo Fisher Scientific, USA) to evaluate the cellular fluorescence indicating uptake of the unconjugated and Aβ-conjugated dyes.

Lactate dehydrogenase (LDH) activity cytotoxicity assay

The cytotoxicity of the PTXG and RODO dyes were evaluated with LDH assay per manufacturers protocol (CyQUANT LDH Cytotoxicity Assay; Thermo #C20300). Briefly, 5000 BV2 cells/100 μL were seeded onto the wells of a 96-well flat bottom plate (Falcon) for 16 hours (overnight). The next day, the cells were treated with the PTXG and RODO dyes (25, 12.5, 6.25, 3.125, 1.56, 0.78, and 0.39 μM) for 24 hours. Cells without any dye treatment were used as a negative control (to measure the spontaneous LDH activity). Cells treated with the provided lysis buffer were used as the positive controls (to measure the maximum LDH activity that is later set to 100%). The % cytotoxicity of the PTXG and RODO dyes were calculated per the equation below and the data was plotted for $n = 3$ biological replicates, mean + sd.

were captured at 30 minute time intervals for 24 hours. The fluorescence intensity, cell confluence, and the integrated fluorescence intensity data were obtained and analyzed using the GraphPad Prism software.

The Aβ^{PH} uptake was measured as the phagocytic score metric, defined as a normalized value relative to the initial fluorescence intensity at $t = 0$ and calculated as:

$$\text{Phagocytic score} = \frac{\text{relative total intensity}(t)}{\text{maximum relative total integrated intensity}}$$

where, relative total integrated intensity (t) is defined as total integrated intensity (t) − total integrated intensity ($t = 0$) for each concentration and cell type.

The total integrated intensity is defined as the total sum of Aβ^{PH} fluorescence intensity in the entire image and given by the expression $\left(\frac{CU \times \mu m^2}{\text{Image}}\right)$ as defined by Incucyte. We captured 4 images per well with multiple replicates for each Aβ^{PH} concentration and for each cell type. These images were used to calculate the value of total integrated intensity, $\left(\frac{CU \times \mu m^2}{\text{Image}}\right)$. The individual units are defined as: CU = average mean intensity (the average of the Aβ^{PH}'s mean fluorescence intensity in each cell in an image), μm^2 = average area (the average area of the Aβ^{PH}'s in each cell in an image).

The maximum relative total integrated intensity is the maximum value of relative total integrated intensity over the 24 hour period. Such a normalization gives phagocytic score values between 0 and 1 to compare different concentrations across different cell types. The maximum peak indicates the time when the degradation is equal to the uptake for each concentration and cell type. All other values show an interplay between uptake or degradation compared to time, $t = 0$, shown by either increase or decrease in florescence that is also observed visually. The corresponding videos (Movies S1–S3†) during live cell

$$\% \text{ cytotoxicity} = \frac{[\text{PTXG or RODO-treated LDH activity} - \text{spontaneous LDH activity}]}{[\text{maximum LDH activity} - \text{spontaneous LDH activity}]}$$

Phagocytosis assay with live microglia

Cells were seeded at 5000 cells per well (200 μL per well) in a 96-well flat bottom plate (Falcon) for approximately 16 hours (overnight). For all cell assays, the lyophilized Aβ^{PH} conjugate was dissolved in the culture medium to prepare a stock solution and was pre-aggregated by placing the stock solution at 37 °C for 24 hours. Further dilution for cell treatment was performed in culture media and the diluted solution was filtered using a 0.22 μm syringe filter prior to cell treatment. The adherent cells (BV2, N9, HMC3) were treated with a final concentration of Aβ^{PH} at a final concentration of 0, 0.1, 0.5, 1.0, 2.0, and 5.0 μM by replacing one-half of the culture medium (100 μL) with a stock Aβ^{PH} solution at 2× concentration. Two technical replicates were used for each treatment concentration. The plates were immediately placed in an IncuCyte S3 Live-Cell Analysis System (Essen BioScience) and four images per well

imaging were taken on IncuCyte S3 Live-Cell Analysis System (Essen BioScience) and stabilized using the Blender version 2.82a software (https://www.blender.org).

Effect of bafilomycin-A1 (BF) on fluorescence of Aβ^{PH} in cells

BV2 cells were seeded at a concentration of 50 000 cells/500 μL media per well in a 12-well flat bottom plate (Falcon) for 16 hours (overnight). The next day, the media was aspirated, and the cells were treated with 400 nM bafilomycin (BF) and placed in a 37 °C incubator for 1 hour. After this time period, the solution was removed and replaced with media containing 100 nM of Aβ^{PH} with or without 400 nM BF for 1 hour. Finally, this solution was removed and the cells were detached from the plates using ice-cold 1× PBS with gentle pipetting. Three minutes before the analysis of each sample, DAPI was added (0.1 μg mL^{-1} cell suspension) to stain for dead cells. The

fluorescence of $A\beta^{PH}$ in the cells were analyzed by flow cytometry (Attune NxT, Thermo Fisher Scientific, USA). Briefly, at least 80% of the total cells were first gated on SSC-A vs. FSC-A plot and the single cells within this gate were selected on the FSC-H vs. FSC-A plot. From the single cells, the live (DAPI −ve) and dead cells (DAPI +ve) were identified. Finally, $A\beta^{PH+}$ or $A\beta^{PH-}$ cells were identified within the live cell population in the $A\beta^{PH+}$ histogram plot. The data was plotted as median fluorescence intensity (MFI) relative to MFI of $A\beta^{PH}$ only for $n = 2$ biological replicates (Fig. S10†).

Isolation and culture of primary mouse microglia

$CD11b^+$ primary microglia were isolated from adult mice aged around 7 months (male and female) and cultured as follows. Mice were euthanized with CO_2 following the Purdue University Animal Care and Use Committee guidelines and brains were transcardially perfused with ice-cold PBS. The perfused brains were dissected and cut into small 1 mm^3 pieces before homogenizing them in Dulbecco's Phosphate Buffered Saline^{++} (i.e. with Ca^{2+} and Mg^{2+} ions) containing 0.4% DNase I on a tissue dissociator (Miltenyi Biotec) at 37 °C for 35 min. The cell suspension was filtered through a 70 μm filter and myelin was removed two times, first using Percoll PLUS reagent followed by myelin removal beads using LS columns (Miltenyi Biotec). After myelin removal, $CD11b^+$ cells were selected from the single cell suspension using the CD11b beads (Miltenyi Biotec) as per the manufacturer's instructions. The $CD11b^+$ cells were finally resuspended in microglia growth media made in DMEM/F12 (Corning Cat. #MT15090CV), further diluted in TIC (TGF-β, IL-34, and cholesterol) media[40] with 2% FBS before seeding 0.1 × 10^6 cells per 500 μL in a well of a 24-well plate (Corning Cat. #353847). The cells were maintained in TIC media at 37 °C and 10% CO_2 with media change every other day until the day (around 10–14 div) of the phagocytosis assay (around 10–14 div).

Flow cytometry analysis of BV2 and primary microglial phagocytosis

BV2 microglial cells were seeded at a density of 250k cells per well in a 6-well plate for around 14 hours overnight. The next morning, the cells were treated with 0.5 μM and 5 μM $A\beta^{PH}$ and placed in a 37 °C incubator for 1 hour, after which the plate was brought to the hood, placed on ice to stop phagocytosis, and cell culture medium containing $A\beta^{PH}$ was aspirated. The cells were washed once with cold PBS. Next, the cells were treated with ice cold PBS containing 2 mM EDTA for 2 minutes on ice to detach the cells from the wells. The cells were then centrifuged at 1400 rpm for 3 minutes. The supernatant was aspirated, and the cell pellets were re-suspended in FACS buffer (PBS, 25 mM HEPES, 2 mM EDTA, and 2% FBS). Five minutes before analysis of each sample, propidium iodide (PI; Thermo Fisher Scientific, Cat. #P1304MP) was added to the sample (40 ng mL^{-1} cell suspension) for staining of dead cells. Phagocytosis of $A\beta^{PH}$ by primary microglial cells was analyzed on div 10–14 in a similar manner. Cells were treated with $A\beta^{PH}$ for 1 hour and detached from the plate using cold PBS and 2 mM EDTA. After centrifuging the cell suspension, the cell pellet was resuspended in

0.1 mL PBS for live/dead staining. Here, Zombie Violet, ZV, (BioLegend, #423113) was used to evaluate cell viability (1 : 100 per 10^6 cells in 0.1 mL) for 15 min followed by PBS wash. Finally, the cells were resuspended in FACS buffer and taken for analysis. Cells exhibiting green fluorescence were captured on the FITC channel upon gating for live cells on Attune NxT flow cytometer (Invitrogen). The files were then analyzed on FlowJo V10 software. Briefly, at least 90% of the total cells were first gated on SSC-A vs. FSC-A plot and the single cells within this gate were selected on the FSC-H vs. FSC-A plot. From the single cells, the live and dead cells were identified from the viability dye. PI^- and ZV^- cells were considered as live cells and PI^+ and ZV^+ cells were taken as dead cells on the histogram plots. Finally, $A\beta^{PH+}$ or $A\beta^{PH-}$ cells were identified within the live cell population in the $A\beta^{PH}$ histogram plot on the FITC channel.

Confocal imaging of actin filaments and nuclei in the paraformaldehyde-fixed phagocytic microglial cells

For labeling the cells with phalloidin and DAPI, 20 000 cells/250 μL were plated in 14 mm microwells of 35 mm glass bottom dishes (MatTek #P35G-1.5-14-C) and kept overnight. The cells were treated with 5.0 μM $A\beta^{PH}$ for 2 hours on the next day. Then the medium was aspirated, and cells were fixed with 4% paraformaldehyde for 20 minutes, and then gently washed once with PBS. Phalloidin-iFluor 594 reagent (Abcam, Cat. #ab176757; 1000× stock) was diluted to 1× in PBS and added to the fixed cells for 10 minutes for staining the actin filaments. To label the nuclei, DAPI was diluted to a concentration of 1 μg mL^{-1}. The cells were washed again with PBS followed by a 10 minute incubation with the diluted DAPI solution. Finally, the DAPI solution (Invitrogen, Cat. #D3571) was aspirated and the fixed cells treated with 2–3 drops of ProLong Gold Antifade Mountant (Invitrogen #P36930) before imaging. Fluorescence images of phagocytic microglial cells were captured using 40× and 60× objectives on a Nikon AR-1 MP confocal laser microscope. Images were obtained using the NIS Elements microscope imaging software.

Confocal imaging of intracellular acidic organelles and nuclei in paraformaldehyde-fixed phagocytic microglial cells

LysoTracker Red DND-99 (Thermo Fisher Scientific, Cat. #L7528) was used for labeling the intracellular organelles of the cells to observe the subcellular localization of $A\beta^{PH}$ sensors inside the cells after phagocytosis. 20 000 cells/250 μL were plated in 14 mm microwells of 35 mm glass bottom dishes (MatTek #P35G-1.5-14-C) and kept overnight. The cells were treated with 5.0 μM $A\beta^{PH}$ for 2 hours on the next day. Then the $A\beta^{PH}$-containing medium was aspirated and replaced with 200 μL of media containing 100 nM concentration of the Lyso-Tracker dye and the cells were incubated in a 37 °C, 5% CO_2 incubator for 30 minutes. Finally, the cells were fixed and treated with DAPI to stain the nuclei followed by 2–3 drops of ProLong Gold Antifade Mountant using the above-mentioned protocol. Fluorescence images of phagocytic microglial cells were captured using 40× and 60× objectives on a Nikon AR-1 MP confocal laser microscope. Images were obtained using the NIS Elements microscope imaging software.

Intracranial injection of Aβ^{PH}, perfusion and immunohistochemistry

Lyophilized Aβ^{PH} was dissolved in Hank's Balanced Salt Solution (HBSS no calcium, no magnesium, no phenol red, ThermoFisher #14175079) to obtain a 100 μM stock solution that was then briefly vortexed and sonicated in a bath sonicator for 1 minute and used immediately for intracranial injections or stored at −80 °C. For intracranial injections, the stock solution was diluted in HBSS to obtain a 10 μM working solution and kept on ice to prevent aggregation. Postnatal day 7 mice were anesthetized with isoflurane and were mounted on a stereotaxic frame. Two lots of 250 nL of Aβ^{PH} working solution were unilaterally injected in the somatosensory cortex of wild-type C57BL/6J mice using a Nanoliter Injector (anteroposterior −2.3 mm; mediolateral +2.3 mm; dorsoventral −0.5 mm for lower layers and −0.2 mm for upper layers, relative to Lambda) at an injection rate of 100 nL min^{-1} followed by 2 additional minutes to allow diffusion. 24 or 72 hours after injections, animals were deeply anesthetized with sodium pentobarbital by intraperitoneal injection and then transcardially perfused with PBS 1× followed by 4% paraformaldehyde (PFA) in PBS. Brains were dissected out, post-fixed for two hours at 4 °C, and cryoprotected in a 30% sucrose-PBS solution overnight at 4 °C. Then, tissue was sectioned at 40 μm on a sliding microtome (Leica). Free-floating brain sections were permeabilized by incubating with 0.3% Triton X-100 in PBS for 1 hour and then blocked for 3 hours (0.3% Triton X-100 and 10% normal donkey serum), followed by incubation with primary antibodies in 0.3% Triton X-100 and 10% normal donkey serum overnight at 4 °C. The next day, brains were rinsed in PBS 1× for 1 hour, incubated with the appropriate secondary antibodies for 2 hours at room temperature, rinsed again in PBS, incubated with DAPI and mounted using Fluoromount-G (SouthernBiotech, #0100-01). During perfusion and immunohistochemistry all solutions were maintained at neutral pH. The following primary antibodies were used: mouse anti-GFAP (1 : 200, Sigma #G3893-100UL) and rabbit anti-IBA1 (1 : 500, Wako Chemicals, #019-1974). The secondary antibodies used were donkey anti-mouse-IgG1 647 (Invitrogen, #A21241) and donkey anti-rabbit 594 (ThermoFisher, #A-21207). Tissue samples were imaged on a ZEISS Axio Imager and a ZEISS LSM 800 confocal using a 20× objective. Aβ^{PH} fluorescence signal was quantified using ImageJ. First, cell contour was manually drawn using IBA1 or GFAP signal and mean fluorescence intensity in the Aβ^{PH} channel was measured. Next, the selection was moved to a nearby region with no obvious Aβ^{PH} fluorescence signal and mean fluorescence intensity in the Aβ^{PH} channel was measured (background). Normalized fluorescence intensity for each cell was calculated as Aβ^{PH} fluorescence signal minus background. Data were analyzed by one-way ANOVA followed by the Sidak's post hoc analysis for comparisons of multiple samples using GraphPad Prism 7 (GraphPad Software).

Immunopanning and culture of primary astrocytes

Astrocytes were purified by immunopanning from the forebrains of P5 Sprague Dawley rats (Charles River) forebrains and cultured as previously described.[60] In brief, cortices were enzymatically disrupted (using papain) and then mechanically dissociated to produce a single-cell suspension that was incubated on several negative immunopanning plates to remove microglia, endothelial cells and oligodendrocyte lineage cells. Positive selection for astrocytes was with an ITGB5-coated panning plate. Isolated astrocytes were cultured in a defined, serum-free base medium containing 50% neurobasal, 50% DMEM, 100 U mL^{-1} penicillin, 100 μg mL^{-1} streptomycin, 1 mM sodium pyruvate, 292 μg mL^{-1} L-glutamine, 1× SATO and 5 μg mL^{-1} of N-acetyl cysteine. This medium was supplemented with the astrocyte-required survival factor HBEGF (Peprotech, 100-47) at 5 ng mL^{-1}.[60] Cells were plated at 5000 cells per well in 12-well plates coated with poly-D-lysine and maintained at 10% CO_2.

Engulfment assay of Aβ^{PH} by primary astrocytes

Astrocytes were maintained for 1 week in culture and checked for their reactivity state using qPCR[5] before addition of Aβ^{PH}. The cells were treated with 0.5, 1.0, or 2.0 μM Aβ^{PH} and imaged continuously with still images taken every 5 minutes with an IncuCyte S3 System epifluorescence time lapse microscope to analyze engulfed Aβ^{PH} particles. For image processing analysis, we took 9 images per well using a 20× objective lens from random areas of the 12-well plates and calculated the phagocytic index by measuring the area of engulfed Aβ^{PH} particles (fluorescence signal) normalized to the area of astrocytes, using ImageJ.

In vivo retinal engulfment of Aβ^{PH}

P14 Sprague Dawley rats were anaesthetized with 2.5% inhaled isoflurane in 2.0 L O_2 per min. Once non-responsive, animals received a 1 μL intravitreal injection of Aβ^{PH}, or PBS. Retinae were collected for immunofluorescence analyses at 3, 24, and 72 hours. At collection, eyeballs were removed, fixed in 4% PFA overnight, and washed in PBS, and retinae were dissected and whole-mounts placed on silanized glass slides. Retinae were blocked with 10% heat-inactivated normal goat serum for 2 hours at room temperature. Incubation with primary antibodies to GFAP (Dako, A0063, 1 : 5 000) and IBA1 (WAKO, 019-19741, 1 : 500) diluted in 5% goat serum in PBS was followed by detection with AlexaFluor fluorescent secondary antibodies (Thermo, 1 : 1000).

Brain slice experiments

Rats at postnatal day 12 (P12) were sacrificed by cervical dislocation followed by decapitation, and 250 μm sagittal hippocampal slices were prepared on a Leica VT 1200S vibratome at 4 °C in oxygenated solution containing (mM): 124 NaCl, 26 $NaHCO_3$, 2.5 KCl, 1 NaH_2PO_4, 10 glucose, 2 $CaCl_2$, 1 $MgCl_2$, 1 kynurenic acid. Acute slices were allowed to recover for 2.5 hours at room temperature before being transferred to 24-well plates and incubated with 5 μM Aβ^{PH} in HEPES-based aCSF (140 mM NaCl, 10 mM HEPES, 2.5 mM KCl, 1 mM NaH_2PO_4, 10 mM glucose, 2 mM $CaCl_2$, and 1 mM $MgCl_2$) for 1.5 hours at 37 °C. Following incubation, slices were quickly rinsed in cold

phosphate-buffered saline (PBS) and fixed in 4% para-formaldehyde (PFA) for 45 minutes at room temperature. For immunolabeling, slices were permeabilized and blocked in buffer containing 10% horse serum and 0.02% Triton X-100 in PBS for 2 hours at room temperature, followed by incubation with goat anti-IBA1 (Abcam, ab5076) or chicken anti-GFAP (Abcam, ab4674) primary antibodies diluted 1 : 500 in blocking buffer for 12 hours at 4 °C. Following four 10 minute washes in PBS, donkey anti-goat IgG 647 (ThermoFisher, A21447) or donkey anti-chicken IgG 649 (Jackson, 703-495-155) secondary antibodies diluted 1 : 1000 in blocking buffer were applied for 4 hours at room temperature. Finally, slices were incubated in DAPI for 30 minutes, rinsed in PBS and mounted. Imaging was done using a Zeiss LSM700 confocal microscope and a 20× objective, where 10 μm image stacks at 1 μm step interval were acquired. For analysis, the percentage of $A\beta^{pH}$ signal within microglial or astroglial cells was calculated by binarizing the microglia or astrocyte channel, creating a mask and multiplying it by the raw $A\beta^{pH}$ signal. The fluorescence intensity of $A\beta^{pH}$ colocalizing with either cell type mask was then expressed as a percentage of the total $A\beta^{pH}$ signal across the field.

In vivo two-photon microscopy

Adult mice bred on a C57BL/6 background aged ~4–7 months (P123 to P203) were anesthetized using urethane (1.55 g kg^{-1} given intraperitoneally). Adequate anesthesia was ensured by confirming the absence of a withdrawal response to a paw pinch. Body temperature was maintained at 36.8 ± 0.3 °C and eyes were protected from drying by applying polyacrylic acid eye drops (Dr Winzer Pharma). The trachea was cannulated and mice were mechanically ventilated with medical air supplemented with oxygen using a MiniVent (Model 845). A headplate was attached to the skull using superglue and mice were head fixed to a custom-built stage. A craniotomy of approximately 2 mm diameter was performed over the right primary somatosensory cortex, immediately caudal to the coronal suture and approximately 2 to 4 mm laterally from the midline. The dura was removed and 2% agarose in HEPES-buffered aCSF was used to create a well filled with HEPES-buffered aCSF during imaging.

Two-photon excitation was performed using a Newport-Spectraphysics Ti:sapphire MaiTai laser pulsing at 80 MHz, and a Zeiss LSM710 microscope with a 20× water immersion objective (NA 1.0). Fluorescence was evoked using a wavelength of 920 nm. The mean laser power under the objective did not exceed 25 mW. Image stacks were taken in 2 μm depth increments (50–200 μm from the cortical surface) every 1.5 min for approximately 30 minutes. Image stacks were maximum intensity projected in the z-dimension and registered using the StackReg plugin in FIJI. Fluorescent changes in the $A\beta^{pH}$ fluorescence were measured from regions of interest (ROIs) drawn around the soma of cells. Five μM $A\beta^{pH}$ in HEPES-based aCSF was applied to the cortical surface for 10 minutes and then replaced with HEPES-based aCSF. Animals were transcardially perfused with ice-cold PBS followed by 4% PFA in PBS at 1.5 or 3 hours after pH $A\beta^{pH}$ application. Brains were post-fixed in PFA for 12 hours at 4 °C and 100 μm sagittal sections were prepared

using a vibratome. Slices were permeabilized and blocked for 12 hours and incubated with rabbit anti-IBA1 (1 : 500, Synaptic Systems, 234006), rat anti-mouse CD68 (1 : 500, Bio-Rad, MCA1957) or chicken anti-GFAP (1 : 500, Abcam, ab4674) primary antibodies for 24 hours at 4 °C. Following washes in PBS, donkey anti-rabbit IgG 647 (1 : 500, ThermoFisher, A31573), goat anti-rat IgG 647 (1 : 500, ThermoFisher, A21247) or donkey anti-chicken IgG 649 (1 : 300, Jackson, 703-495-155) was applied for 12 hours at 4 °C. Image stacks (23 μm deep) were acquired at 1 μm interval in the cerebral cortex and analysis was done as for in situ experiments.

Funding sources

Data availability

All data supporting this article have been included as part of the ESI.

Author contributions

Priya Prakash: conceptualization, investigation, formal analysis and methodology including all the cell lines and primary cells experiments, writing – original draft, writing – review & editing. Krupal P. Jethava: conceptualization, investigation, formal analysis and methodology including development of probes and chemical characterization, writing – original draft, writing – review & editing. Nils Korte: methodology, investigation, formal analysis including *in vivo* 2-photon assessment of glial uptake and data analysis, writing – review & editing. Pablo Izquierdo: methodology, investigation, formal analysis of glia in hippocampal slices and imaging and data analysis, writing – review & editing. Emilia Favuzzi: methodology, investigation including stereotaxic injections and data analysis. Indigo VL Rose: methodology, investigation including retinal injection and astrocyte experiments. Kevin A Guttenplan: methodology, investigation including astrocyte experiments. Palak Manchanda: methodology, investigation. Sayan Dutta: methodology. Jean-Christophe Rochet: resources, supervision. Gord Fishell: resources, supervision. Shane A Liddelow: methodology, resources, supervision, writing – review & editing. David Attwell: methodology, resources, supervision, writing – review & editing. Gaurav Chopra: conceptualization, funding acquisition, methodology, project administration, resources, supervision, writing – original draft, writing – review & editing.

Conflicts of interest

Shane Liddelow is an academic founder of AstronauTx Ltd. Other authors declare no competing financial interests.

Acknowledgements

References

1 J. B. Zuchero and B. A. Barres, *Development*, 2015, **142**, 3805–3809.

2 Q. Li and B. A. Barres, *Nat. Rev. Immunol.*, 2018, **18**, 225–242.

3 A. Nimmerjahn, F. Kirchhoff and F. Helmchen, *Science*, 2005, **308**, 1314–1318.

4 A. D. Bachstetter, L. J. Van Eldik, F. A. Schmitt, J. H. Neltner, E. T. Ighodaro, S. J. Webster, E. Patel, E. L. Abner, R. J. Kryscio and P. T. Nelson, *Acta Neuropathol. Commun.*, 2015, **3**, 32.

5 S. A. Liddelow, K. A. Guttenplan, L. E. Clarke, F. C. Bennett, C. J. Bohlen, L. Schirmer, M. L. Bennett, A. E. Münch, W.-S. Chung, T. C. Peterson, D. K. Wilton, A. Frouin, B. A. Napier, N. Panicker, M. Kumar, M. S. Buckwalter, D. H. Rowitch, V. L. Dawson, T. M. Dawson, B. Stevens and B. A. Barres, *Nature*, 2017, **541**, 481–487.

6 A. F. Lloyd and V. E. Miron, *Nat. Rev. Neurol.*, 2019, **15**, 447–458.

7 M. L. Hanke and T. Kielian, *Clin. Sci.*, 2011, **121**, 367–387.

8 E. Okun, M. P. Mattson and T. V Arumugam, *NeuroMol. Med.*, 2010, **12**, 164–178.

9 J. Husemann, J. D. Loike, R. Anankov, M. Febbraio and S. C. Silverstein, *Glia*, 2002, **40**, 195–205.

10 S. Hong and B. Stevens, *Dev. Cell*, 2016, **38**, 126–128.

11 J. Canton, *J. Leukoc. Biol.*, 2014, **96**, 729–738.

12 N. M. Wakida, G. M. S. Cruz, C. C. Ro, E. G. Moncada, N. Khatibzadeh, L. A. Flanagan and M. W. Berns, *PLoS One*, 2018, **13**(4), e0196153.

13 W.-S. Chung, L. E. Clarke, G. X. Wang, B. K. Stafford, A. Sher, C. Chakraborty, J. Joung, L. C. Foo, A. Thompson, C. Chen, S. J. Smith and B. A. Barres, *Nature*, 2013, **504**, 394–400.

14 J. Doherty, M. A. Logan, O. E. Tasdemir and M. R. Freeman, *J. Neurosci.*, 2009, **29**, 4768–4781.

15 Y. Fuentes-Medel, M. A. Logan, J. Ashley, B. Ataman, V. Budnik and M. R. Freeman, *PLoS Biol.*, 2009, 7(8), e1000184.

16 Y. M. Morizawa, Y. Hirayama, N. Ohno, S. Shibata, E. Shigetomi, Y. Sui, J. Nabekura, K. Sato, F. Okajima, H. Takebayashi, H. Okano and S. Koizumi, *Nat. Commun.*, 2017, **8**, 28.

17 R. Nortley, N. Korte, P. Izquierdo, C. Hirunpattarasilp, A. Mishra, Z. Jaunmuktane, V. Kyrargyri, T. Pfeiffer, L. Khennouf, C. Madry, H. Gong, A. Richard-Loendt, W. Huang, T. Saito, T. C. Saido, S. Brandner, H. Sethi and D. Attwell, *Science*, 2019, **365**, eaav9518.

18 M. Lei, H. Xu, Z. Li, Z. Wang, T. T. O'Malley, D. Zhang, D. M. Walsh, P. Xu, D. J. Selkoe and S. Li, *Neurobiol. Dis.*, 2016, **85**, 111–121.

19 C. Sato, N. R. Barthélemy, K. G. Mawuenyega, B. W. Patterson, B. A. Gordon, J. Jockel-Balsarotti, M. Sullivan, M. J. Crisp, T. Kasten, K. M. Kirmess, N. M. Kanaan, K. E. Yarasheski, A. Baker-Nigh, T. L. S. Benzinger, T. M. Miller, C. M. Karch and R. J. Bateman, *Neuron*, 2018, **97**, 1284–1298.e7.

20 J. M. Long and D. M. Holtzman, *Cell*, 2019, **179**, 312–339.

21 M. T. Heneka, M. J. Carson, J. El Khoury, G. E. Landreth, F. Brosseron, D. L. Feinstein, A. H. Jacobs, T. Wyss-Coray, J. Vitorica, R. M. Ransohoff, K. Herrup, S. A. Frautschy, B. Finsen, G. C. Brown, A. Verkhratsky, K. Yamanaka, J. Koistinaho, E. Latz, A. Halle, G. C. Petzold, T. Town, D. Morgan, M. L. Shinohara, V. H. Perry, C. Holmes, N. G. Bazan, D. J. Brooks, S. Hunot, B. Joseph, N. Deigendesch, O. Garaschuk, E. Boddeke, C. A. Dinarello, J. C. Breitner, G. M. Cole, D. T. Golenbock and M. P. Kummer, *Lancet Neurol.*, 2015, **14**, 388–405.

22 R. J. O'Brien and P. C. Wong, *Annu. Rev. Neurosci.*, 2011, **34**, 185–204.

23 D. J. Selkoe, *Neuron*, 1991, **6**(4), 487–498.

24 G. Krabbe, A. Halle, V. Matyash, J. L. Rinnenthal, G. D. Eom, U. Bernhardt, K. R. Miller, S. Prokop, H. Kettenmann and F. L. Heppner, *PLoS One*, 2013, **8**, e60921.

25 A. M. Floden and C. K. Combs, *J. Alzheimers. Dis.*, 2011, **25**, 279–293.

26 H. Sarlus and M. T. Heneka, *J. Clin. Invest.*, 2017, **127**, 3240–3249.

27 P. D. Wes, I. R. Holtman, E. W. G. M. Boddeke, T. Möller and B. J. L. Eggen, *Glia*, 2016, **64**, 197–213.

28 R. S. Jones, A. M. Minogue, T. J. Connor and M. A. Lynch, *J. Neuroimmune Pharmacol.*, 2013, **8**, 301–311.

29 J. Koenigsknecht and G. Landreth, *J. Neurosci.*, 2004, **24**, 9838–9846.

30 S. Ribes, S. Ebert, D. Czesnik, T. Regen, A. Zeug, S. Bukowski, A. Mildner, H. Eiffert, U.-K. Hanisch, S. Hammerschmidt and R. Nau, *Infect. Immun.*, 2009, **77**, 557–564.

31 S. Hassan, K. Eldeeb, P. J. Millns, A. J. Bennett, S. P. H. Alexander and D. A. Kendall, *Br. J. Pharmacol.*, 2014, **171**, 2426–2439.

32 D. M. Paresce, R. N. Ghosh and F. R. Maxfield, *Neuron*, 1996, **17**, 553–565.

33 L. D. Lavis, T. J. Rutkoski and R. T. Raines, *Anal. Chem.*, 2007, **79**, 6775–6782.

34 pHrodo™ Red, https://assets.thermofisher.com/TFS-Assets/LSG/manuals/mp36600.pdf.

35 L. Ma, Q. Ouyang, G. C. Werthmann, H. M. Thompson and E. M. Morrow, *Front. Cell Dev. Biol.*, 2017, **5**, 71.

36 C. Mauvezin and T. P. Neufeld, *Autophagy*, 2015, **11**, 1437–1438.

37 P. Prakash, T. C. Lantz, K. P. Jethava and G. Chopra, *Methods Protoc.*, 2019, **2**, 48.

38 W. B. Stine, L. Jungbauer, C. Yu and M. J. Ladu, *Methods Mol. Biol.*, 2011, **670**, 13–32.

39 W. B. Stine, K. N. Dahlgren, G. A. Krafft and M. J. LaDu, *J. Biol. Chem.*, 2003, **278**, 11612–11622.

40 C. J. Bohlen, F. C. Bennett, A. F. Tucker, H. Y. Collins, S. B. Mulinyawe and B. A. Barres, *Neuron*, 2017, **94**, 759–773.e8.

41 S. Liu, Y. Liu, W. Hao, L. Wolf, A. J. Kiliaan, B. Penke, C. E. Rube, J. Walter, M. T. Heneka, T. Hartmann, M. D. Menger and K. Fassbender, *J. Immunol.*, 2012, **188**, 1098–1107.

42 Y. Liu, S. Walter, M. Stagi, D. Cherny, M. Letiembre, W. Schulz-Schaeffer, H. Heine, B. Penke, H. Neumann and K. Fassbender, *Brain*, 2005, **128**, 1778–1789.

43 Y. Zhao, X. Wu, X. Li, L.-L. Jiang, X. Gui, Y. Liu, Y. Sun, B. Zhu, J. C. Piña-Crespo, M. Zhang, N. Zhang, X. Chen, G. Bu, Z. An, T. Y. Huang and H. Xu, *Neuron*, 2018, **97**, 1023–1031.e7.

44 S. Parhizkar, T. Arzberger, M. Brendel, G. Kleinberger, M. Deussing, C. Focke, B. Nuscher, M. Xiong, A. Ghasemigharagoz, N. Katzmarski, S. Krasemann, S. F. Lichtenthaler, S. A. Müller, A. Colombo, L. S. Monasor, S. Tahirovic, J. Herms, M. Willem, N. Pettkus, O. Butovsky, P. Bartenstein, D. Edbauer, A. Rominger, A. Ertürk, S. A. Grathwohl, J. J. Neher, D. M. Holtzman, M. Meyer-Luehmann and C. Haass, *Nat. Neurosci.*, 2019, **22**, 191–204.

45 G. Kleinberger, Y. Yamanishi, M. Suarez-Calvet, E. Czirr, E. Lohmann, E. Cuyvers, H. Struyfs, N. Pettkus, A. Wenninger-Weinzierl, F. Mazaheri, S. Tahirovic, A. Lleo, D. Alcolea, J. Fortea, M. Willem, S. Lammich, J. L. Molinuevo, R. Sanchez-Valle, A. Antonell, A. Ramirez, M. T. Heneka, K. Sleegers, J. van der Zee, J.-J. Martin, S. Engelborghs, A. Demirtas-Tatlidede, H. Zetterberg, C. Van Broeckhoven, H. Gurvit, T. Wyss-Coray, J. Hardy, M. Colonna and C. Haass, *Sci. Transl. Med.*, 2014, **6**, 243ra86.

46 T. A. Siddiqui, S. Lively, C. Vincent and L. C. Schlichter, *J. Neuroinflammation*, 2012, **9**, 770.

47 O. E. Tasdemir-Yilmaz and M. R. Freeman, *Genes Dev.*, 2014, **28**, 20–33.

48 J. Nuutila and E.-M. Lilius, *Cytometry, Part A*, 2005, **65**, 93–102.

49 C.-W. Chow, G. P. Downey and S. Grinstein, *Curr. Protoc. Cell Biol.*, 2004, **22**, 15.7.1–15.7.33.

50 O. Butovsky, M. P. Jedrychowski, C. S. Moore, R. Cialic, A. J. Lanser, G. Gabriely, T. Koeglsperger, B. Dake, P. M. Wu, C. E. Doykan, Z. Fanek, L. Liu, Z. Chen, J. D. Rothstein, R. M. Ransohoff, S. P. Gygi, J. P. Antel and H. L. Weiner, *Nat. Neurosci.*, 2014, **17**, 131–143.

51 Q. Xiao, P. Yan, X. Ma, H. Liu, R. Perez, A. Zhu, E. Gonzales, J. M. Burchett, D. R. Schuler, J. R. Cirrito, A. Diwan and J.-M. Lee, *J. Neurosci.*, 2014, **34**, 9607–9620.

52 J. A. Fernández-Albarral, E. Salobrar-García, R. Martínez-Páramo, A. I. Ramírez, R. de Hoz, J. M. Ramírez and J. J. Salazar, *J. Optom.*, 2019, **12**, 198–207.

53 A. Gomez-Arboledas, J. C. Davila, E. Sanchez-Mejias, V. Navarro, C. Nuñez-Diaz, R. Sanchez-Varo, M. V. Sanchez-Mico, L. Trujillo-Estrada, J. J. Fernandez-Valenzuela, M. Vizuete, J. X. Comella, E. Galea, J. Vitorica and A. Gutierrez, *Glia*, 2018, **66**, 637–653.

54 C. Ruan, L. Sun, A. Kroshilina, L. Beckers, P. De Jager, E. M. Bradshaw, S. A. Hasson, G. Yang and W. Elyaman, *Brain. Behav. Immun.*, 2020, **83**, 180–191.

55 W. J. Streit, N. W. Sammons, A. J. Kuhns and D. L. Sparks, *Glia*, 2004, **45**, 208–212.

56 W. J. Streit, H. Braak, Q. S. Xue and I. Bechmann, *Acta Neuropathol.*, 2009, **118**, 475–485.

57 D. Guneykaya, A. Ivanov, D. P. Hernandez, V. Haage, B. Wojtas, N. Meyer, M. Maricos, P. Jordan, A. Buonfiglioli, B. Gielniewski, N. Ochocka, C. Cömert, C. Friedrich, L. S. Artiles, B. Kaminska, P. Mertins, D. Beule, H. Kettenmann and S. A. Wolf, *Cell Rep*, 2018, **24**, 2773–2783.e6.

58 A. Mildner, B. Schlevogt, K. Kierdorf, C. Böttcher, D. Erny, M. P. Kummer, M. Quinn, W. Brück, I. Bechmann, M. T. Heneka, J. Priller and M. Prinz, *J. Neurosci.*, 2011, **31**, 11159–11171.

59 S. A. Grathwohl, R. E. Kälin, T. Bolmont, S. Prokop, G. Winkelmann, S. A. Kaeser, J. Odenthal, R. Radde, T. Eldh, S. Gandy, A. Aguzzi, M. Staufenbiel, P. M. Mathews, H. Wolburg, F. L. Heppner and M. Jucker, *Nat. Neurosci.*, 2009, **12**, 1361–1363.

60 L. C. Foo, N. J. Allen, E. A. Bushong, P. B. Ventura, W.-S. Chung, L. Zhou, J. D. Cahoy, R. Daneman, H. Zong, M. H. Ellisman and B. A. Barres, *Neuron*, 2011, **71**, 799–811.